2025, Scienceline Publication
World's Veterinary Journal
World Vet J, 15(2): 341-374.
ISSN 2322-4568

DOI: https://dx.doi.org/10.54203/scil.2025.wvj37
PII: S232245682500037-15

Immunoinformatics Approach to Develop a Novel Chimeric L1/L2 Messenger RNA-based Vaccine Targeting a Broad Spectrum of Human Papillomavirus Species

Nshimiyimana Sylvere[1]*, James Kimotho[2], and Caroline Wangari Ngugi[3]

[1]*Department of Molecular Biology and Biotechnology, Pan African University Institute for Basic Sciences, Technology and Innovation, Nairobi P.O. Box 62000-00200, Kenya*
[2]*Innovation and Technology Transfer Department, Kenya Medical Research Institute, Nairobi P.O. Box 54840-00200, Kenya*
[3]*Department of Medical Microbiology, Jomo Kenyatta University of Agriculture and Technology, Nairobi P.O. Box 62000-00200, Kenya*

*Corresponding author's Email: sylvere.nshimiyimana@students.jkuat.ac.ke

ORIGINAL ARTICLE
Received: March 29, 2025
Revised: April 27, 2025
Accepted: May 28, 2025
Published: June 25, 2025

ABSTRACT

Papillomaviruses can infect animals and humans, causing benign lesions and cancer. Chimeric vaccines may address the limited coverage of current papillomavirus vaccines by providing cross-type immunity. The present study focused on the *in silico* design of a chimeric mRNA vaccine targeting a wide range of human papillomaviruses (HPV). The study incorporated 25 amino acid sequences derived from L1 and L2 capsid proteins of 14 high-risk and 11 low-risk HPV strains. These sequences underwent multiple sequence alignment, and the resulting sequences were used to develop consensus sequences. Computational approaches were then applied to predict and identify immunodominant T-cell and B-cell epitopes. The mRNA vaccine structure was designed by merging codon-optimized multi-epitope chimeric peptides with regulatory components that enhance both transcription and translation efficiency. The present study identified 19 T and 6 B cell epitopes, which were evaluated as non-toxic, non-allergenic, highly antigenic, and fully or partially conserved. The final multi-epitope peptide vaccine had a molecular weight of 60,161.29 kDa, a theoretical isoelectric point (pI) of 9.44, a solubility index of 0.451, and an antigenicity score of 0.9178. The mRNA vaccine exhibited a stable mRNA structure with a minimum free energy of -731.10 kcal/mol and an estimated molecular weight of 644.98 kDa. The proposed vaccine demonstrated no cross-affinity with the human genome and attained a worldwide population coverage rate of 86.24%. The vaccine formed a stable docking complex and exhibited strong interactions with major histocompatibility class I and class II molecules, as well as Toll-like receptor 4 (TLR4), Toll-like receptor 9 (TLR9), and the B-cell receptor. Binding affinities were assessed based on free energy (ΔG) values of -34.01 kcal/mol and -20.77 kcal/mol for major histocompatibility complex (MHC) class I and II, respectively, -1377.5 kcal/mol for TLR4, -24.19 kcal/mol for TLR9, and -34.41 kcal/mol for the B-cell receptor. This vaccine triggered both antibody and cell-mediated immune responses and increasing levels of IFN-γ and the interleukins IL-2, IL-10, and IL-12. This vaccine is considered preventive against multiple HPV infections. Nonetheless, *in vitro* and *in vivo* investigations are necessary to validate the safety and efficacy of this vaccine.

Keywords: Chimeric mRNA, Immune simulation, Molecular docking, Molecular dynamics simulation, Multi-epitope peptides, Papillomavirus

INTRODUCTION

Human papillomaviruses (HPV) are responsible for 99% of cervical cancer, 93% of anal cancer, 40% of vaginal cancer, 40% of penile cancer, 63% of oropharyngeal cancer, 51% of vulvar cancer, and can also lead to head and neck malignancies (Mahmoudvand et al., 2022). The primary way that HPVs are spread is through intercourse with an infected person. According to reports from 2020, cervical cancer is a significant global health challenge, ranking as the fourth most frequent cancer among women globally, with an approximation of 604,127 new cases and a fatality rate of 341,831 (Singh et al., 2023). This disease is most common in Africa, with 119,000 new cases and a mortality rate of 69,000, as reported in 2018 (Jedy-Agba et al., 2020). By contrast, Sub-Saharan Africa has an average of 24% of the world's high-risk HPV infection rates; Southeast Asia (14%) and Eastern Europe (14%) next, followed by Latin America and the Caribbean (16%) (Bruni et al., 2010; Jedy-Agba et al., 2020).

Cervical cancer is associated with 14 high-risk human papillomaviruses (HR-HPV), such as HPV 16, 18, 31, 33, 35, 39, 45, 51, 52, 56, 58, 59, 66, and 68 (Haręża et al., 2022), as well as intermediates, potentially carcinogenic types, causing approximately 2% of cases of cervical cancer, comprising HPV26, 30, 34, 53, 66, 67, 69, 70, 73, and 82 (Geraets et al., 2012). It has been reported 23 low-risk (LR-HPV) variants, such as 6, 11, 26, 40, 42, 53, 54, 55, 61, 62, 64, 67, 69, 70, 71, 72, 73, 81, 82, 83, 84, IS39, and CP6108 that are non-carcinogenic or cause benign anogenital or cutaneous warts (Serretiello et al., 2023). The two main causes of cervical cancer globally are HPV-16 and HPV-18, which account for 270,000 fatalities, with developing nations accounting for 85% of these cases (Ahmed et al., 2017), and with an

To cite this paper: Sylvere N, Kimotho J, and Ngugi CW (2025). Immunoinformatics Approach to Develop a Novel Chimeric L1/L2 Messenger RNA-based Vaccine Targeting a Broad Spectrum of Human Papillomavirus Species. *World Vet. J.*, 15(2): 341-374. DOI: https://dx.doi.org/10.54203/scil.2025.wvj37

estimated $8.0 billion in medical expenses per year (Chesson et al., 2012). In contrast, infections caused by HPV have been reported not only in humans but also in birds and reptiles. Researchers have identified 24 canine papillomaviruses (CPVs) and six feline papillomaviruses (FcaPVs), linked to different oral and cutaneous illnesses in dogs and cats (Medeiros-Fonseca et al., 2023). Currently, there are restrictions on commercial vaccinations for bovine papillomavirus (BPV) and canine oral papillomavirus (COPV), which frequently rely on L1-based virus-like particles (VLPs) (Jagu et al., 2011). Nevertheless, these vaccinations may lack extensive cross-protection against different HPV strains. The use of L2 in chimeric designs is anticipated to enhance cross-protection, as it contains conserved regions shared among different HPV types (Li et al., 2016). This approach may therefore offer a more effective strategy for veterinary applications.

All HPVs possess capsids, which are non-enveloped icosahedral viruses (T = 7d) with a diameter of 55-60 nm. These viruses include a double-stranded DNA genome comprising late segments (L), which include two late genes (L1 and L2) that play a role in virion assembly and entry (Haręża et al., 2022). This genome also includes early proteins (E), comprising six early genes (E1, E2, E4, E5, E6, E7), which promote viral replication, and a long control region (LCR), which functions as the viral origin of replication and regulates transcription (Wang, 2015). Currently, the US food and drug administration (FDA) has approved three primary prophylactic HPV vaccines including bivalent (Gardasil-9, 9vHPV), which offers protection against nine HPV types (6, 11, 16, 18, 31, 33, 45, 52, and 58); quadrivalent (Gardasil, 4vHPV), which targets HPV types 6, 11, 16, and 18; and bivalent HPV vaccine (Cervarix, 2vHPV), which protects against HPV types 16, 18, and 45 (Boxus et al., 2016; Huber et al., 2021).

These vaccines, which are L1-based, have demonstrated strong immunogenicity, safety, and effectiveness. However, the protection they offer is restricted to particular HPV types that they are intended to target. Furthermore, these vaccines do not produce broad-spectrum neutralizing immunity against other HPV types, suggesting that certain non-targeted HPV genotypes persist in propagating infection (Akuzum et al., 2018). To address these challenges, recent advancements in HPV L2-based vaccination have focused on achieving both broad-spectrum and type-specific protection against a range of HPV genotypes (Ryan et al., 2024).

Despite L2-based vaccinations offering great potential, they have been demonstrated to elicit only modestly enhanced immune responses compared to L1 virus-like particles (VLPs) (Kristi et al., 2017). Therefore, the development of fusion or chimeric vaccines via co-expression of major (L1) and minor (L2) capsid proteins constitutes a feasible method for generating multivalent vaccines with improved immunogenicity.

Epitope prediction is a computational method for designing multi-subunit vaccines for emerging infections. This field uses specific pathogen components, known as epitopes, to create vaccines (Sanami et al., 2023). Epitope-based peptide vaccine development simplifies the design process, making it cheaper and quicker; choosing immunodominant epitopes determines what triggers an immune response (Cai et al., 2021). The *in silico* approach and bioinformatics strategies, including computational tools, techniques, and databases, have been employed to develop effective vaccine candidates aimed at combating numerous human pathogenic diseases, including viruses like SARS-CoV-2 and mammarenavirus (Shawan et al., 2023), HPV infection (Mahmoudvand et al., 2022; Sanami et al., 2023), and monkeypox virus (Sanami et al., 2023).

In recent years, mRNA technology has been utilized to develop preventive vaccines against infectious diseases. Wolff et al. (1990) demonstrated the initial *in vitro*-transcribed mRNA-expressing reporter proteins in muscle post-injection and noted that mRNA encoding viral or pathogenic antigens provoked immunological responses against the specific antigen (Maruggi et al., 2019). The mRNA-based technology is gaining traction in vaccine development because of its rapid manufacturing process, and is considered non-infectious due to the lack of genome mutation, and it promotes both humoral and cell-mediated immunity (Maruggi et al., 2019).

In the present study, an in silico technique was used to predict epitopes from fourteen high-risk (14HR-HPV) and eleven low-risk (11 LR-HPV) of major capsids (L1) and minor capsids (L2) proteins. The consensus sequences, derived from the highly conserved amino acid sequences at each site, were used to predict epitopes following the multiple sequence alignment (MSA) of 25 protein sequences. The present study aimed to design a chimeric L1/L2 mRNA-based vaccine targeting a broad range of HPV genotypes. All successful epitopes were connected with the necessary linkers, and this construct was used to build an mRNA structure to create a multi-epitope chimeric L1/L2 mRNA-based vaccine.

MATERIALS AND METHODS

Ethical approval

This research was entirely based on immunoinformatics and computational analyses. No animal or human subjects were involved in the design or execution of this study.

***In silico* procedures and essential steps**

The immuno-informatics flow chart for developing a chimeric L1/L2 mRNA-based vaccine against diverse HPV species in this study (Figure 1A and 1B).

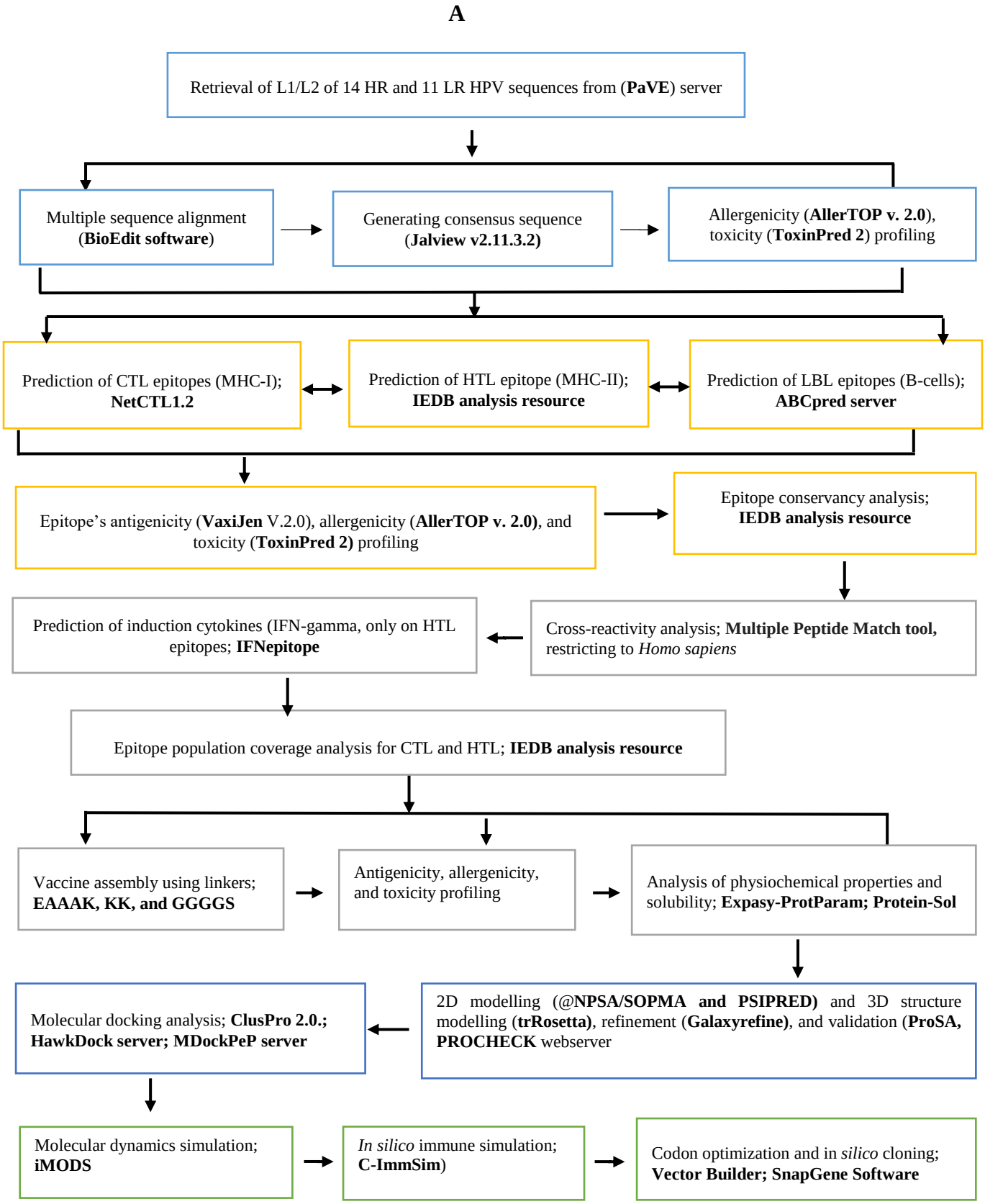

Figure 1A. Depicts an overview of all *in silico* procedures

B

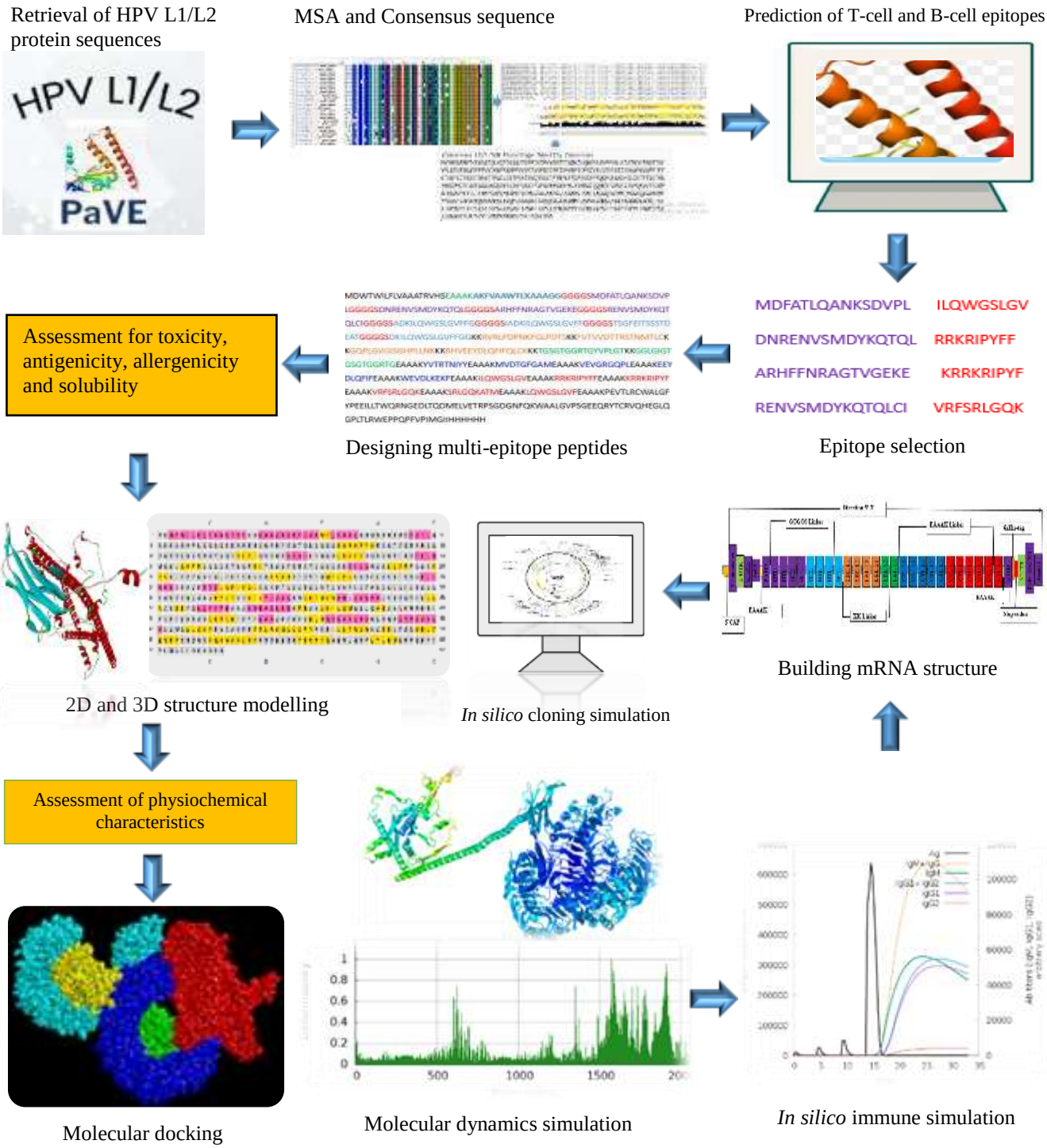

Figure 1B. Highlights the crucial steps involved in *in silico* procedures

Retrieval of protein sequence, identification of conserved regions, and generation consensus sequences

The present study encompassed 25 amino acid sequences chosen from 14 high-risk (HR) and 11 low-risk (LR) HPV types (Haręża et al., 2022; Serretiello et al., 2023). In each category, the chosen HPV types were derived from highly carcinogenic HR and LR varieties associated with benign vaginal warts or epithelial lesions. The major (L1) and minor (L2) capsid proteins of HPV were included in these sequences. These sequences were obtained from the PaVE database and utilized as input for the upcoming bioinformatics analysis. The BioEdit program (version 7.0) was used to perform multiple sequence alignments on protein sequences using the ClustalW algorithm. The alignment results were then uploaded into the Jalview software v2.11.3.2) to generate consensus sequences, which were then used to predict putative immunogenic T and B cell epitopes (Waterhouse et al., 2009). Figures 2A and 2C display the multiple sequence alignment (MSA) of the chosen HPV strains and their accession numbers.

Immune cell epitope prediction (T cells and B cells)

Cytotoxic T lymphocyte (CTL) cells recognize endogenous antigenic peptides presented by major histocompatibility complex (MHC) I molecules. In contrast, helper T lymphocyte (HTL) cells recognize foreign antigenic peptides presented by MHC II molecules (Shi et al., 2024). The T cells are incapable of directly recognizing epitopes; they must engage with MHC molecules to identify antigen-presenting cells (APCs) (Sha et al., 2020; Shi et al., 2024). In the context of antigen presentation, MHC molecules are predominantly categorized into two types, including class I (MHC I) and class II (MHC II) (Rock et al., 2016). The epitopes for MHC class I were predicted utilizing the NetCTL-1.2 online tools (Larsen et al., 2007). The method combines the prediction of peptide MHC class I binding, proteasomal C-terminal cleavage, and TAP transport efficacy. The server facilitates predictions of CTL epitopes constrained to the 12 MHC class I supertypes. Artificial neural networks are utilized for MHC class I binding and proteasomal cleavage. The transport efficiency of TAP is predicted with a weight matrix. Prediction parameters were configured to default settings for peptide length (9-mer peptides, with a weight on C-terminal cleavage of 0.15, a weight on TAP transport efficiency of 0.05, and an epitope identification threshold of 0.75. Furthermore, criteria were established to integrate MHC, cleavage, and TAP transport (Larsen et al., 2007).

The Immune Epitope Database (IEDB) analytic tools were used to predict epitopes for MHC-class II, or HTL (Jensen et al., 2018). The parameters were established by default, selecting species/locus as (Human, HLA-DR), utilizing the complete human leucocyte antigen (HLA) reference set with a panel of 27 alleles that offer over 99% population coverage for MHC II (Dehghani et al., 2024), and employing netMHCIIpan 4.1 EL (recommended epitope predictor 2023.09) as the predictive methodology. The ABC Pred server was used to assess linear B Cell Lymphocyte (BCL) epitopes. ABCPred utilizes ANN scores to rank epitopes based on scores surpassing the threshold of 0.5; a sequence with a higher score is more likely to be an epitope. Consequently, the epitope prediction was established at a threshold score of 0.81. This program predicts linear B cell (LBL) epitopes of 15 amino acids with an accuracy of 65.93%, employing a recurrent neural network (Saha and Raghava, 2007). Discontinuous B-cell epitopes or non-linear B-cell epitopes are essential components of an antibody. Predicting discontinuous B-cell epitopes is crucial for creating vaccines that accurately replicate natural antigenic structures and generate robust, specific antibody responses (Ponomarenko et al., 2008). The non-linear B-cell epitopes were identified from the refined three-dimensional (3D) model utilizing the online Elli-Pr program, accessible on the IEDB server. The parameters for epitope prediction were established with a maximum score of 0.5 and a maximum distance of 6 Ångströms.

Screening the best epitopes for toxicity, antigenicity, allergenicity, and evaluation of vaccine physiochemical characteristics and solubility

Non-toxic epitopes were assessed utilizing the ToxPred2 web server, utilizing batch submission and protein scanning as criteria. The server functions with the SVM (Swiss-Prot) algorithm (Gupta et al., 2013). The VaxiJen v2.0 was employed to assess the antigenicity of the predicted epitopes by selecting viral organisms as target species and establishing a threshold of ≥ 0.4 (Hasan et al., 2024). The service demonstrates an accuracy of 70-89% in predicting tumor, viral, and bacterial antigens. Aller-TOP v2.1 was employed to assess the allergenicity of the predicted epitopes (Dimitrov et al., 2014). This service categorizes epitopes as "potential allergens" and "potential non-allergens. Protein solubility was analyzed using the Protein-Sol server (Hebditch et al., 2017). The ExPASy-ProtParam tool was utilized to assess the vaccine's physicochemical properties (Naveed et al., 2022).

Epitope human homology and conservation analysis

Epitope conservation, a crucial step in the immunoinformatics methodology, determines the degree of desirable epitope distributions within the homologous protein ensemble. The epitope conservancy analysis tool from the IEDB was employed to determine the conservancy percentage by examining the identities of protein sequences (Hasan et al., 2024).

Analysis of the population coverage of cytotoxic T lymphocyte and helper T lymphocyte epitopes

The geographic distribution of HLA alleles differs globally. Consequently, to maximize individual outreach, population coverage must be considered in the development of a successful vaccine candidate (Shawan et al., 2023). The population coverage tool on the IEDB server utilizes MHC binding and/or T-cell restriction data to ascertain the coverage of certain CTL and HTL epitopes across class I, class II, and their combination. The examination of CTL and HTL population coverage was based on the identification of epitopes by global human leucocyte antigen (HLA).

Prediction of helper T lymphocyte-inducing cytokines

Type II interferon-gamma (IFN-γ) enhances antigen presentation by upregulating MHC molecules, hence augmenting T-cell responses (Shao et al., 2017). Moreover, IFN-γ prolongs T-cell memory, which is crucial for the long-term effectiveness of vaccines (Pulendran et al., 2021). They also improve antigen presentation in macrophages and dendritic cells (APCs), which improves immune responses (Shao et al., 2017). The induction of cytokines for HTL epitopes was investigated using the IFNepitope web server, which applies SVM-based methodologies and models for comparing IFN with other cytokines (Castro et al., 2018).

Designing an mRNA-based vaccine

The final, top-ranked epitopes, such as CTL, HTL, and LBL, were combined using amino acid linkers to build a chimeric L1/L2 vaccine model, following the methods described by Kakakhel et al. (2023) and Oladipo et al. (2022).

The chimeric mRNA vaccine construct was designed by arranging selected epitopes in a specific order to optimize immunogenicity and coverage. The sequence begins with helper T lymphocyte (HTL) epitopes, followed by linear B-cell (LBL) epitopes, and ends with cytotoxic T lymphocyte (CTL) epitopes. Specifically, it consists of 4 HTL epitopes from L1 and 4 from L2, then 4 LBL epitopes from L1 and 2 from L2, and finally 5 CTL epitopes from L1 and 6 from L2. The KK linker was used to join intra-B cell epitopes, while EAAAK and GGGGS were used to combine intra-CTL and HTL epitopes, respectively. Furthermore, the EAAAK linker was used to link the IgE signal peptide and PADRE sequence. The ultimately chosen top-ranked epitopes, including CTL, HTL, and LBL, were amalgamated utilizing amino acid linkers to construct a chimeric L1/L2 vaccine model. The KK linker facilitated the conjunction of intra-B cell epitopes, whilst EAAAK and GGGGS were employed to amalgamate intra-CTL and HTL epitopes, respectively. Additionally, the EAAAK linker was employed to connect the IgE signal peptide to the PADRE sequence.

The N-terminal of this vaccine design had a Pan-DR-binding epitope (PADRE: AKFVAAWTLKAAAGG) and the IgE leader signal peptide (MDWTWILFLVAAATRVHS). PADRE was incorporated as a universal synthetic peptide that binds to the MHC-II receptor, activating CD4+ T-cells and initiating an innate immunological response, while also functioning as a Toll-like receptor agonist (Ghaffari-Nazari et al., 2015). The PADRE can be synergistically integrated with TLR agonists in vaccine formulation, enhancing robust helper T-cell activation and resulting in superior adaptive immune responses (Rosa et al., 2004). The IgE signal leader peptide was incorporated into the vaccine design to guide newly synthesized antigenic proteins to the endoplasmic reticulum for proper folding and secretion. In the C-terminal, the vaccine contained MITD (UniProt ID: Q5S1P3) to direct MHC class I epitopes to the endoplasmic reticulum and a 6xHis-tag for detection and purification purposes (Oladipo et al., 2022). The linkers were used to ensure that the proteins maintain a stable and flexible conformation. To optimize mRNA design for *in vitro* transcription and subsequent translation, essential regulatory elements were integrated into the construct. These included a T7 promoter to drive *in vitro* transcription, 5′ and 3′ untranslated regions (UTRs) derived from α- and β-human globin, respectively, a Kozak consensus sequence (GCCGCCACCATGGCG) to enhance translational initiation, a poly (A) tail consisting of 120 adenosine residues (A), a translation termination codon, and a BspQI restriction site for precise plasmid linearization. The inclusion of these elements is consistent with established methodologies aimed at improving mRNA stability and translational efficiency (Pichon and Perche, 2021). UTRs were provided by GenScript.

Modelling of two and three-dimensional (2D and 3D) structures, refining, and validating the vaccine candidate

The SOPMA tool and PSIPRED 4.0 were employed to predict the conformational states (alpha-helix, beta-sheet, turn, coil) of the vaccine design (Hasan et al., 2024). The trRosetta web server was utilized to generate the 3D structure of the vaccine. This server employs a limited trRosetta methodology to develop the protein structure via direct energy minimization, utilizing inter-residue distance and orientation distributions predicted by a deep neural network (Du et al., 2021). The 3D model was optimized to improve structural integrity via the Galaxyrefine server. The quality assessment was corroborated by the Pro-SA online platform, PROCHECK, and ERRAT, which were utilized for stereochemistry analysis via the Ramachandran plot (Sanami et al., 2023).

Analysis of molecular docking

A vaccine design may have the potency to elicit an immune response against a varying number of epitopes recognized by the HLA alleles. For this reason, the most frequent MHC class I/II alleles were selected from RCSB PDB using the PDB accession codes (PDB ID: 6TDS) and (PDB ID: 1BX2), respectively. Epitopes were screened by a molecular docking method with MHC class I and II alleles using the MDockPeP server (Xu et al., 2018). A molecular docking study was conducted to demonstrate the interaction of the proposed vaccine with Toll-like receptors (TLR4 and TLR9), MHC alleles, and B-cell receptors (BCRs). The ClusPro server v2.0 was employed to dock vaccine-TLR4, whereas the HawkDock server v2 was utilized to analyze interactions involving vaccine-TLR9, MHC class I/II, and BCR receptors. HawkDock was employed to assess binding interactions, determine binding free energy, and execute Molecular Mechanics Generalized Born Surface Area (MM-GBSA) analysis. Toll-like receptors (TLR4 and TLR9) are proteins that engage with antigens from diverse organisms, initiating immune responses such as cytokine production (Kaur et al., 2022). The PDB ID codes for human TLR4, TLR9, and BCR receptors are 3FXI, 8AR3, and CD79 (PDB ID: 3KG5), respectively. These receptors were downloaded from the Protein Data Bank (RCSB PDB). The Dock Prep server, an integrated tool in the UCSF Chimera v1.17.3 software, was used to prepare the receptors. Instead, the constructed vaccine was treated as a ligand. The preparation of receptors consisted of removing co-crystallized ligands, heteroatoms, and water molecules. The next step involved adding hydrogen GM (Gasteiger-Marsili) charges (Shawan et al., 2023). The LigPlot+DIMPLOT and PDBsum server programs were used to determine the interaction between the ligand (vaccine) and receptors.

Simulating molecular dynamics of the docking complex

The molecular dynamics simulation (MD) approach plays a crucial role in determining the atomic behavior and interactions of other biomolecules based on interatomic forces (Hollingsworth and Dror, 2018). The internal coordinate normal mode analysis server (iMODS) was utilized to examine the interatomic dynamics between the vaccine and receptor complexes (López-Blanco et al., 2014). This program forecasts intricate torsional angles, examines protein and nucleic acid dynamics through normal mode analysis (NMA), structural deformation, eigenvalues, root mean square deviation (RMSD), covariance, and complex stability.

***In silico* immune simulation**

Immunomodeling forecasts the immune system's recognition of epitope peptides. The graphs of the simulation and the epitope outcomes were generated by the C-IMMSIM Online server. This immune server utilizes machine learning (AI) and a position-specific scoring matrix (PSSM) to predict epitopes and study immune interactions (Rapin et al., 2011). The simulation volume was kept at the default parameters. Four injections were set as a time step for injection scheduled on days 1, 14, 28, and 42 (The first dose was given at time = 0, and each time-step equals 8 hours of real life) with several antigens to inject, optimized to 20, 50, 100, and 1000. All other parameters were configured to their default values, including 100 simulation steps, a random seed of 12345, host HLA selection, a vaccine without LPS, an adjuvant value of 100, and the simulation volume of 10.

Codon optimization, secondary structure prediction for mRNA vaccine, and cloning simulation

Codon optimization was performed using the Vector-Builder's Codon Optimization program, specifically designed for humans (*Homo sapiens*; Liu et al., 2021). This program optimizes gene expression by picking codons favored in human cells. The optimized sequences can enhance protein yields and overall expression levels in experimental applications. The generated sequence was then cloned into a standard cloning vector provided by GenScript (pUC57) using SnapGene software, flanked by EcoRI and SacI restriction enzymes. The final mRNA construct was generated utilizing the optimized DNA sequence from the Codon Optimization tool provided by Vector Builder. The DNA sequence was subsequently uploaded to the RNAfold web server to forecast the secondary structure of the mRNA vaccine construct. This server forecasts mRNA structures utilizing the least free energy and partition algorithm, assigning a minimal free energy (MFE) score to evaluate the MFE of secondary and centroid structures (Gruber et al., 2008).

RESULTS

Retrieval of protein sequences, multiple sequence alignment, and generating consensus sequences

Twenty-five amino acid sequences were selected from high-risk and low-risk HPV types derived from the major (L1) and minor (L2) capsid proteins. BioEdit software version 7.0.0 performed the multiple sequence alignments (MSA) (Figures 2A and 3C) and Jalview version 2.11.3.2 generated the consensus sequences. The consensus sequence was generated from the highly conserved amino acid residues at each position to facilitate the development of an effective vaccine against multiple types (Figures 2B and 3D).

Prediction and evaluation of major histocompatibility class I and II (MHC-I/II) and Linear B CELL (LBL) epitopes based on L1/L2 proteins

The study employed NetCTL 1.2 servers to categorize immunogenic epitopes according to MHC class I. The IEDB server was utilized to predict Helper T cell epitopes using human leukocyte alleles (MHC class II; HLA-DR) as the species or locus, NetMHCIIpan 4.1 EL as the prediction method, and a 15-mer epitope length. Analysis of CTL L1 epitopes revealed that, of the 45 potential CTL epitopes, only 11.11% (5 out of 45) successfully met the criteria for toxicity, antigenicity, allergenicity, and conservancy (Table 1). Similarly, 48 potential CTL epitopes derived from L2 proteins were selected. Only 26.7% (13 of 48) of epitopes successfully passed the screening for toxicity, antigenicity, and allergenicity. Of the 13 subjects, 46.15% (6 out of 13) exhibited conservation level and were selected for vaccine design (Table 2).

The IEDB server identified 53 MHC-II binding epitopes derived from L1 proteins. Following screening, 16.98% (9 of 53) of HTL epitopes, deemed non-toxic, non-allergenic, and probable antigens. However, 44.4% (4 out of 9) of the epitopes incorporated in the vaccine design exhibited conservation based on conservation analysis and were retained (Table 1). The prediction of HTL from L2 proteins led to the discovery of 38 possible epitopes using the IEDB server. However, only 10.5% (4 of the 38) were likely to be antigens and were not toxic or allergenic. These 4 epitopes, as predicted by epitope conservation analysis (IEDB Analysis Resource), were retained for vaccine design (Table 2)

B-cell epitopes play a crucial role in antigenic determinants and are detected by B-cell receptors (BCR). The ABCpred server predicts linear B-cell (LBL) epitopes, which are 15 amino acids in length, using a recurrent neural network. Using a threshold of 0.81, 31 potential linear B-cell lymphocyte (LBL) epitopes derived from L1 proteins were identified. Out of 31, 25.8% (8 out of 31) were found to be non-toxic, probable antigens, and non-allergens. The IEDB conservancy analysis indicated that 22.22% (4 out of 18) of the epitopes were conserved and selected for vaccine design (Table 1). Furthermore, 37 linear B-cell epitopes derived from L2 proteins were predicted. The assessment for antigenicity, allergenicity, and toxicity revealed that 48.64% (18 out of 37) of the LBL epitopes were non-toxic, non-allergenic, and probable antigens. Only two epitopes that demonstrated conservation through the conservancy analysis method were retained for further examination (Table 2). The present study included epitopes that were entirely or partially conserved and successfully underwent screening for toxicity, antigenicity, and allergenicity.

The present study evaluated the capacity of selected HTL epitopes to induce IFN-γ cytokine production using an *in silico* method with the IFNepitope server. The results revealed four HTL L1 epitopes and four HTL L2 epitopes that produced IFN-γ with favorable scores (Table 3).

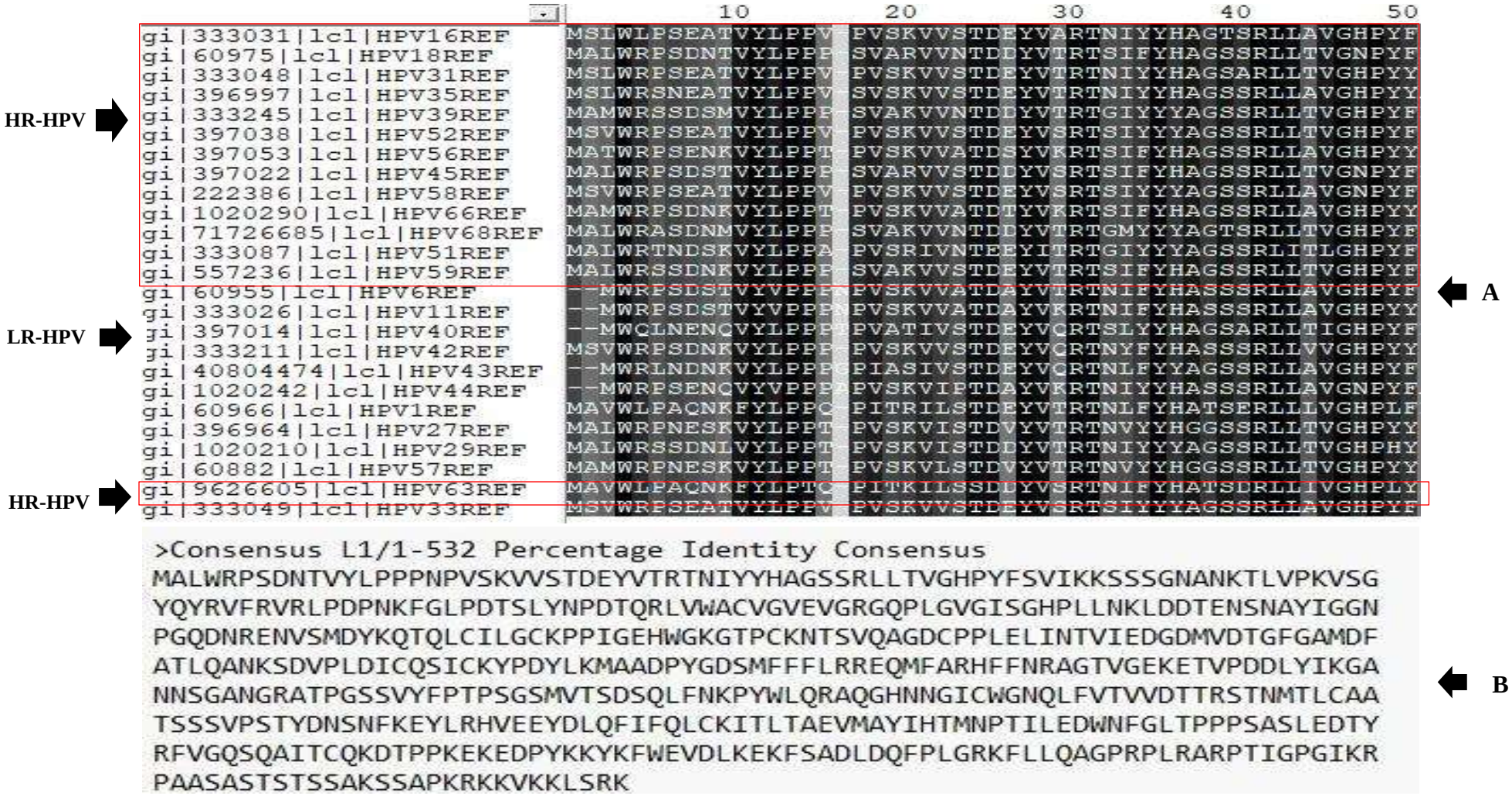

Figure 2. Multiple sequence alignment and consensus sequences derived from human papillomavirus (L1) proteins. **A**: Depicts a multiple sequence alignment of 25 protein sequences, comprising 14 high-risk (sequences enclosed within the red rectangular frame) and 11 low-risk (non-enclosed sequences) human papillomavirus (HR-HPV and LR-HPV) strains. **B**: The produced consensus sequence. BioEdit software version 7.0.0 conducted multiple sequence alignment, while Jalview version 2.11.3.2 produced the consensus sequence.

To cite this paper: Sylvere N, Kimotho J, and Ngugi CW (2025). Immunoinformatics Approach to Develop a Novel Chimeric L1/L2 Messenger RNA-based Vaccine Targeting a Broad Spectrum of Human Papillomavirus Species. *World Vet. J.*, 15(2): 341-374. DOI: https://dx.doi.org/10.54203/scil.2025.wvj37

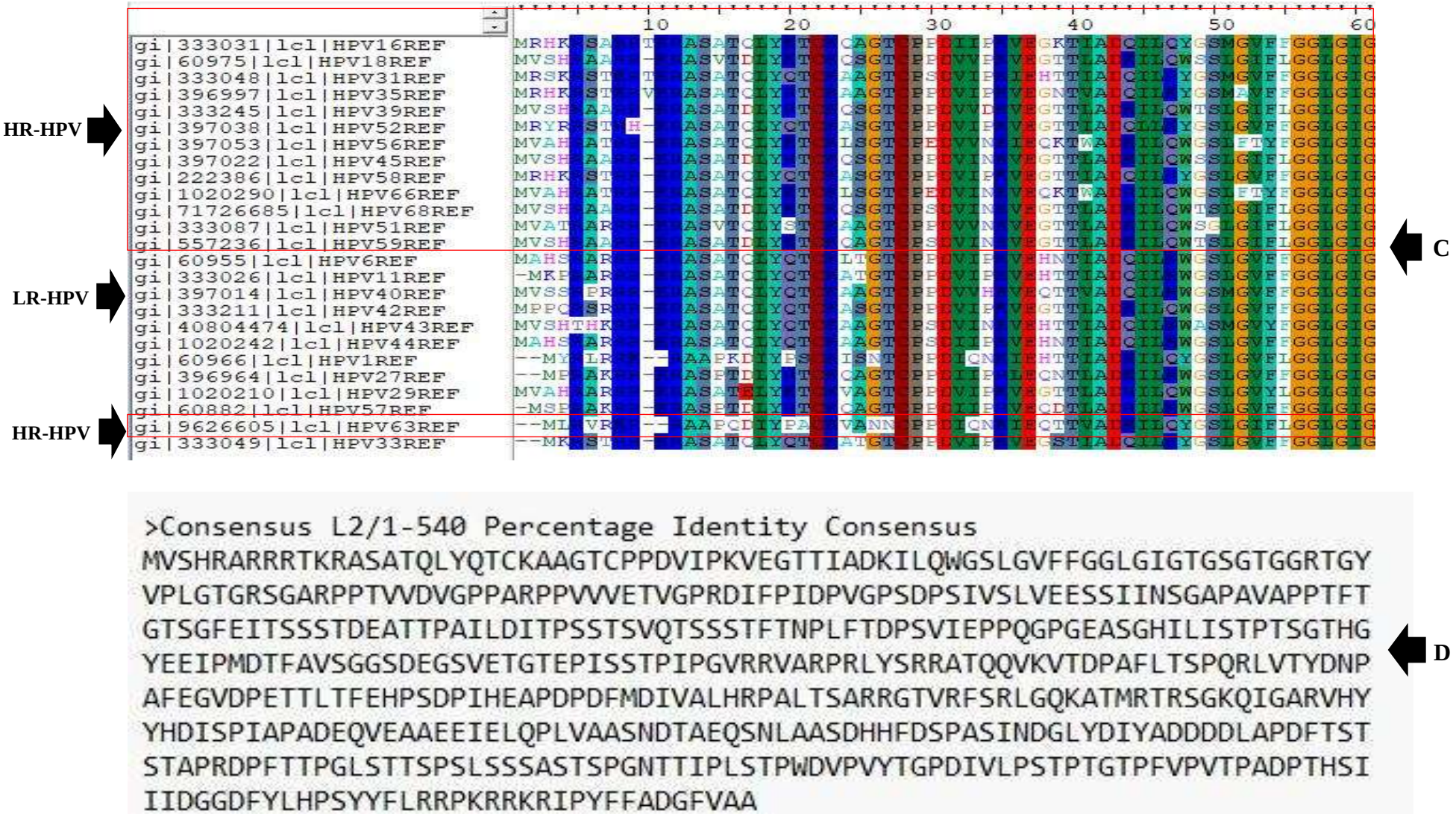

Figure 3. Multiple sequence alignment and consensus sequences derived from human papillomavirus (L2) proteins. **C**: Depicts a multiple sequence alignment of 25 protein sequences, comprising 14 high-risk and 11 low-risk human papillomavirus (HR-HPV and LR-HPV) strains. **D**: The produced consensus sequence. BioEdit software version 7.0.0 conducted multiple sequence alignment, while Jalview version 2.11.3.2 produced the consensus sequence.

Table 1. The L1 (CTL, HTL and LBL [B cell]) epitopes successfully passed screening based on antigenicity, toxicity, allergenicity, and conservancy analysis

Type of epitopes	Allele	Epitope sequence	Antigenicity score at the threshold (≥ 0.4)	Toxicity/allergenicity	Conservancy analysis at the max. identity set to 100%
CTL (5)	HLA-A*01:01,HLA-A*26:01	YVTRTNIYY	0.6843	Non-toxin/allergen	100.00%: HPV31,HPV35,HPV29
	HLA-A*01:01,HLA-A*26:01	MVDTGFGAM	1.6337	Non-toxin/allergen	100.00%:HPV16,HPV31,HPV35,HPV66, HPV6, HPV11, HPV40, HPV43,HPV44
	HLA-B*39:01,HLA-B*40:01	VEVGRGQPL	1.2418	Non-toxin/allergen	100.00%: HPV16, HPV35, HPV39, HPV51, HPV40, HPV27, HPV29, HPV57
	HLA-B*40:01	EEYDLQFIF	1.7384	Non-toxin/allergen	100.00%:HPV16,HPV18,HPV35,HPV39,HPV45,HPV45,HPV68, HPV6, HPV43,HPV27, HPV29, HPV57
	HLA-B*40:01	WEVDLKEKF	1.2621	Non-toxin/allergen	100.00%: HPV35, HPV52, HPV33
HTL (4)	HLA-DRB1*01:01	MDFATLQANKSDVPL	0.7698	Non-toxin/allergen	93.33%
	HLA-DRB1*03:01	DNRENVSMDYKQTQL	1.4352	Non-toxin/allergen	100%: HPV42
	HLA-DRB1*04:05	ARHFFNRAGTVGEKE	0.7295	Non-toxin/allergen	86.67%
	HLA-DRB1*03:01	RENVSMDYKQTQLCI	1.6266	Non-toxin/allergen	93.33%
LBL (4)		FVTVVDTTRSTNMTLC	1.0558	Non-toxin/allergen	100.00%: HPV52, HPV58, HPV6, HPV11, HPV33
		GQPLGVGISGHPLLNK	0.5668	Non-toxin/allergen	100.00%: HPV16, HPV31, HPV35, HPV52, HPV42, HPV44, HPV33
		RHVEEYDLQFIFQLCK	0.4410	Non-toxin/allergen	93.75%
		RVRLPDPNKFGLPDTS	0.4553	Non-toxin/allergen	100.00%: HPV16, HPV31, HPV35, HPV52, HPV42, HPV44, HPV33

CTL (5): Cytotoxic T lymphocytes epitopes, HTL (4): Helper T lymphocytes, LBL (4): Linear B Cell lymphocytes, HPV: Human papillomavirus, HLA: Human leucocyte antigen

Table 2. The L2 (CTL, HTL and LBL [B cell]) epitopes successfully passed screening based on antigenicity, toxicity, allergenicity and conservancy analysis

Type of epitopes	Allele	Epitope sequence	Antigenicity score at the threshold (≥ 0.4)	Toxicity/allergenicity	Conservancy analysis at the max. identity set to 100%
CTL (6)	HLA-A*02:01	ILQWGSLGV	1.8703	Non-toxin/allergen	100.00%: HPV42, HPV29
	HLA-B* 15:01	LQWGSLGVF	2.2096	Non-toxin/allergen	100%: HPV42
	HLA-B*27:05	RRKRIPYFF	1.5931	Non-toxin/allergen	100.00%:HPV35,HPV56,HPV66,HPV1
	HLA-B*27:05	KRRKRIPYF	1.7636	Non-toxin/allergen	100.00%: HPV51
	HLA-B*27:05	VRFSRLGQK	2.1048	Non-toxin/allergen	100.00%: HPV51
	HLA-B*27:05	SRLGQKATM	1.2853	Non-toxin/allergen	100.00%: HPV51
HTL (4)	HLA-DRB1*15:01	ADKILQWGSLGVFFG	0.8722	Non-toxin/allergen	100.00%: HPV42
	HLA-DRB1*15:01	IADKILQWGSLGVFF	0.9813	Non-toxin/allergen	93.33%
	HLA-DRB1*07:01	TSGFEITSSSTDEAT	0.6108	Non-toxin/allergen	73.33%
	HLA-DRB1*15:01	DKILQWGSLGVFFGG	0.6126	Non-toxin/allergen	100.00%: HPV42
LBL (2)		TGSGTGGRTGYVPLGT	1.3789	Non-toxin/allergen	93.75%
		GGLGIGTGSGTGGRTG	1.4744	Non-toxin/allergen	100.00%: HPV16, HPV18, HPV58, HPV59, HPV6, HPV43, HPV44, HPV27, HPV29, HPV 57

CTL (6): Cytotoxic T lymphocytes epitopes, HTL (4): Helper T lymphocytes, LBL (2): Linear B Cell lymphocytes, HPV: Human papillomavirus, HLA: Human leucocyte antigen

Table 3. The predicted cytokines induction for HTL epitopes on L1/L2 proteins

Type of epitopes	Epitope sequence	IFN-γ	IFN-γ score
HTL L1 (4)	MDFATLQANKSDVPL	POSITIVE	0.45234024
	DNRENVSMDYKQTQL	POSITIVE	0.39683519
	ARHFFNRAGTVGEKE	POSITIVE	0.46861774
	RENVSMDYKQTQLCI	POSITIVE	0.50127294
HTL L2 (4)	ADKILQWGSLGVFFG	POSITIVE	0.53283921
	IADKILQWGSLGVFF	POSITIVE	0.53596388
	TSGFEITSSSTDEAT	POSITIVE	0.41927147
	DKILQWGSLGVFFGG	POSITIVE	0.56924381

IFN-γ: Interferon gamma; HTL (4): Helper T lymphocytes

Molecular docking between cytotoxic T lymphocyte epitopes and major histocompatibility class I alleles

The final vaccine design contained 11 CTL epitopes generated from L1/L2 proteins, as they had the lowest docking energy score against the most common MHC-class I alleles worldwide (PDB ID: 6TDS), using the MDockPeP server (Figure 4 and Table 4).

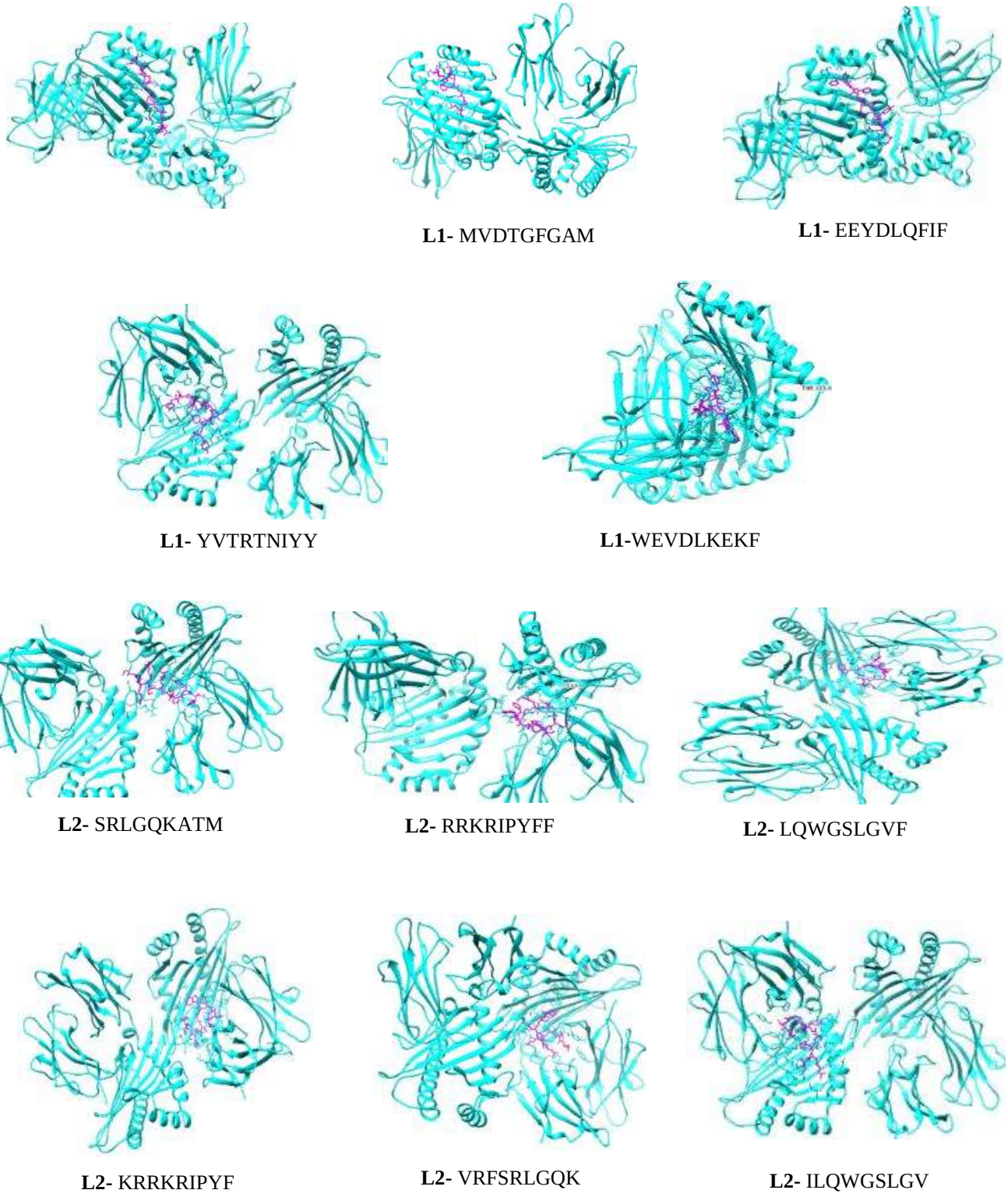

Figure 4. Docking between major histocompatibility class-I alleles and cytotoxic T lymphocyte epitopes produced from L1/L2 proteins. The receptors are indicated in gray, whereas epitope peptides are shown in magenta. The docking complex was visualized with the UCSF Chimera v1.17.3 program.

To cite this paper: Sylvere N, Kimotho J, and Ngugi CW (2025). Immunoinformatics Approach to Develop a Novel Chimeric L1/L2 Messenger RNA-based Vaccine Targeting a Broad Spectrum of Human Papillomavirus Species. *World Vet. J.*, 15(2): 341-374. DOI: https://dx.doi.org/10.54203/scil.2025.wvj37

Table 4. Docking between MHC-I alleles and CTL epitopes produced from L1/L2 proteins

HLA class I Alleles	CTL L1 epitopes	Docking score
PDB ID: 6TDS, HLA-A02:01	VEVGRGQPL	-140.1
	MVDTGFGAM	-143.9
	EEYDLQFIF	-174.1
	WEVDLKEKF	-187.9
	YVTRTNIYY	-205.9
	CTL L2 epitopes	**Docking score**
	KRRKRIPYF	-197.7
	RRKRIPYFF	-204.3
	LQWGSLGVF	-161.0
	ILQWGSLGV	-161.7
	SRLGQKATM	-147.4
	VRFSRLGQK	-177.1

CTL: Cytotoxic T lymphocytes epitopes, HLA: Human leucocyte antigen, MHC-I: Major histocompatibility complex class I, PDB: Protein data bank

Epitope human homology and population coverage analysis

Human epitope homology was employed to identify the most immunogenic and pathogen-specific epitopes, while excluding those that resemble self-proteins. The individual epitope was verified by restricting organisms from UniProt complete proteomes (*Homo sapiens*, taxid: 9606). Not all predicted epitopes were detected in the human genome, indicating that they exhibit no cross-reactivity with the human proteome. The population coverage analysis of combined epitopes L1/L2 proteins (CTL L1 and CTL L2) and (HTL L1 and HTL L2) revealed to cover the majority of Europe (92.93%), followed by North America (88.33 %), East Asia (76.73%), South Asia (75.51%), and North Africa (75.59%). However, the lowest population coverage rates were observed in Central America (21.92%), Central Africa (44.53%), South America (51.7%), and East Africa (53.67%). Overall, the vaccine achieved a global coverage rate of 86.24% (Figure 5). The MHC molecules are extremely variable, with over a thousand known variants, resulting in varying binding specificity to homologous epitopes, which can be related to population coverage scores that vary among ethnicities.

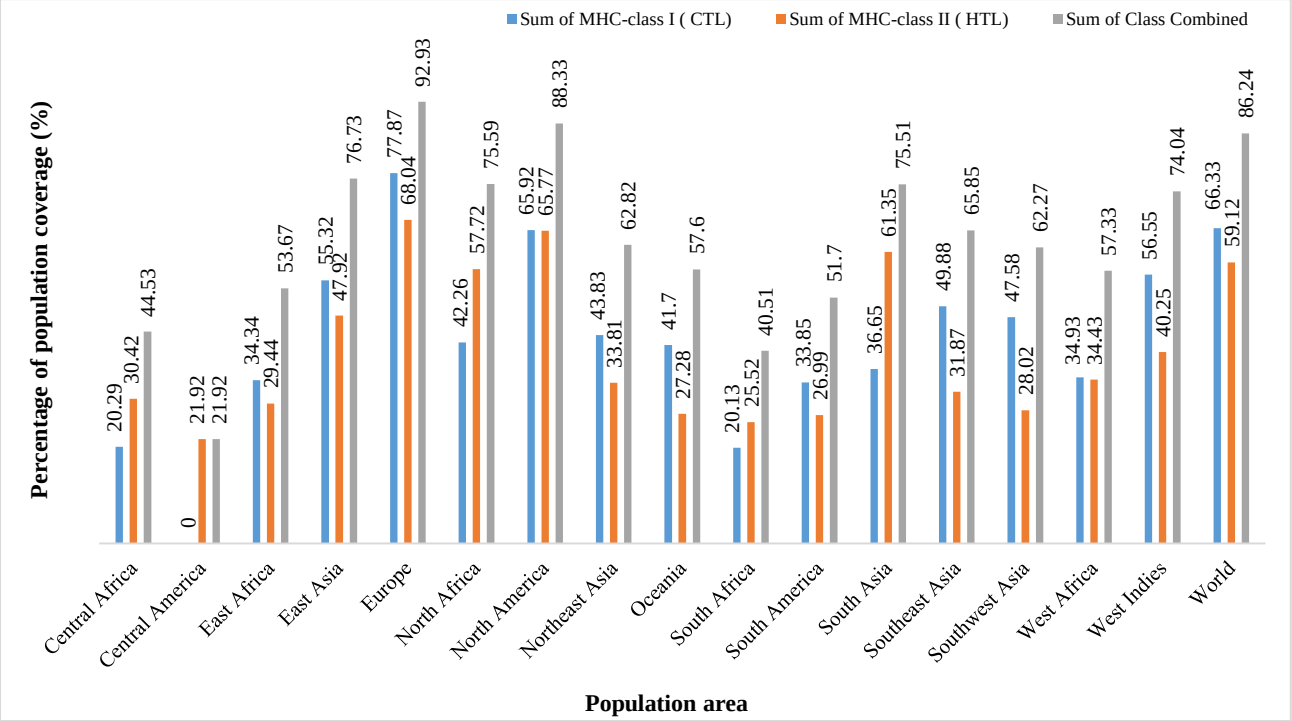

Figure 5. Population coverage calculation of cytotoxic T lymphocyte (CTL) and helper T lymphocyte (HTL) epitopes derived from L1/L2 proteins

Chimeric mRNA-based vaccine assembly

The chimeric L1/L2 mRNA-based vaccine model with 25 epitopes was generated by conjugating various combinations of shortlisted CTL, HTL, and B-cell (LBL) epitopes with appropriate linkers. The chimeric mRNA-based vaccine was composed of 4 HTL L1 and 4 HTL L2 joined together using GGGGS, 4 LBL L1 and 2 LBL L2 linked with a KK flexible linker, and 5 CTL L1 and 6 CTL L2 combined with an EAAAK rigid linker. Other regulatory elements added to the primary construct included the signal peptide (IgE leader sequence), the Pan DR-binding epitope (PADRE),

and MITD (UniProt ID: Q5S1P3) to direct MHC class I epitopes to the endoplasmic reticulum. Moreover, a Histidine (6xHis-tag) was incorporated into the C-terminal for detection and purification purposes. To design a complete mRNA structure, a T7 promoter RNA polymerase (TAATACGACTCAC TATAGGG), 5'UTR (human alpha-globin gene: HBA), and Kozak sequence were added in the N-terminal, while a translation stop signal (a stop codon), 3'UTR (human beta-globin gene: HBB), and Poly (Ax120) tail were added to the C-terminal of the vaccine construct. Moreover, the restriction enzyme (BspQI: GCTCTTC) sequence was added after the Poly (A) tail to facilitate the linearization of plasmid DNA for *in vitro* transcription. UTRs for α-human globin (5'UTR) and β-human globin (3'UTR) were introduced to maintain mRNA stability. Figure 6 shows a graphical representation of a chimeric mRNA-based vaccine construct against diverse HPV species.

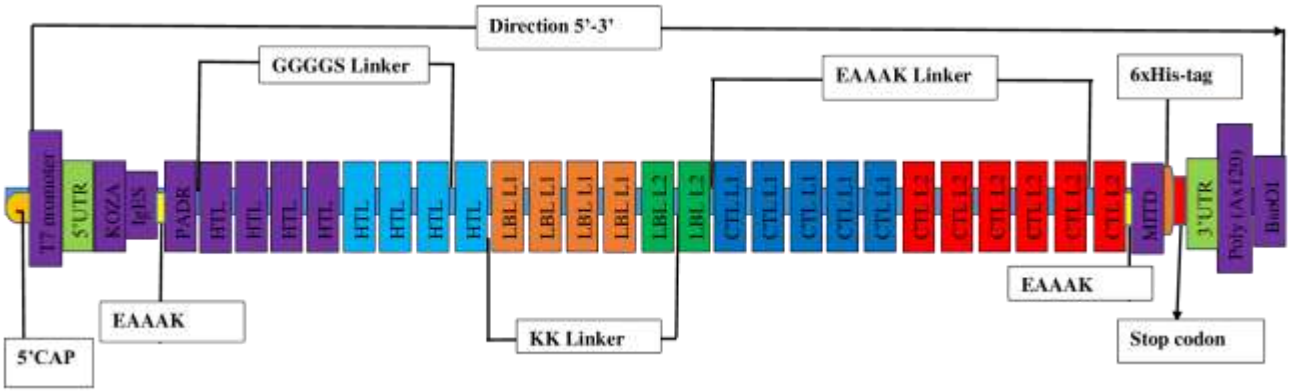

Figure 6. Graphical representation of chimeric L1/L2 mRNA-based vaccine construct against human papillomavirus species. The construct consists of 19 T-cell epitopes and 6 B-lymphocyte epitopes, along with a T7 promoter, 5'unstranslated region (5'UTR) from α-human globin, a 3'UTR from β-human globin (3'UTR), a Kozak sequence, a stop codon, a Poly (Ax120) tail, a 6xHis-Tag sequence, and a plasmid linearization restriction enzyme sequence (BspQI).

Assessment of antigenicity, allergenicity, and solubility profiling and physiochemical properties of the vaccine construct

The ProtParam server estimated the molecular weight of the multi-epitope chimeric peptide vaccine to be 60161.29~60kDa and a theoretical pI of 9.44, suggesting a basic character. Of the 562 amino acid residues, fifty-six (56) were negatively charged (Asp+Glu), while seventy-three (73) were positively charged (Arg+Lys). The vaccine exhibited thermal stability (aliphatic index = 68.49) and a stability rating over 40 (instability index = 36.89). Furthermore, the grand average of hydropathicity (GRAVY) was estimated to be -0.366, indicating a hydrophilic character and illustrating its capacity to interact more effectively with surrounding water molecules. The Protein-Sol service predicted the solubility of the vaccine to be 0.451. A scaled solubility value over 0.45 is anticipated to exhibit increased solubility compared to the average solubility of *E. coli* protein in the experimental solubility dataset by Niwa et al. (2009). Moreover, the vaccine demonstrated an average half-life of 30 hours *in vivo* (in mammalian reticulocytes), exceeding 20 hours in yeast, and surpassing 10 hours in *Escherichia coli*. The vaccine exhibited an antigenicity score of 0.9178 at a threshold of ≥ 0.4 and contained no suspected allergens, as confirmed by the VaxiJen 2.0 and AllerTOP v.2.0 servers, respectively. Table 5 summarizes the physicochemical characteristics of the selected vaccine design, highlighting the vaccine's stability and its ability to elicit a robust immune response in the organism. The vaccine is anticipated to be safe, as allergenicity tests indicated no risk of allergenicity. The examination of physicochemical characteristics revealed that the vaccine structure meets the standards for vaccine formulation (Table 5).

Table 5. Physiochemical properties of the multi-epitope chimeric vaccine construct.

Features	Value
Number of amino acids	562aa
Molecular weight	60161.29~ 60kDa
Theoretical pI	9.44
Solubility (> 0.45)	0.451
Antigenicity score (≥ 0.4)	0.9178
Allergenicity	Non-allergen
Instability index	36.89
Aliphatic index	68.49
Grand average of hydropath city GRAVY)	-0.366
Formula	C2683H4187N761O786S15
Total number of atoms	8432
Estimated half-life	30 hours (mammalian reticulocytes, *in vitro*) > 20 hours (yeast, *in vivo*) > 10 hours (Escherichia coli, *in vivo*)

Secondary (2D) structure prediction of the chimeric L1/L2 mRNA-based vaccine

The 2D structure of the produced vaccine was predicted and validated by applying PSIPRED (Figure 7B) and SOPMA (Figure 7C) servers. SOPMA servers calculate the fraction of 2D configurations using four conformational states, including alpha helix, sheet, turn, and random coil. The secondary structure results revealed that the proposed vaccine had 129 (22.95%) alpha helices, 158 (28.11%) extended strands, and 275 (48.93%) random coils. The outcomes revealed that the designed vaccine had acceptable configuration states of protein characterized by flexibility and stability, which indicated that epitopes are located in an accessible region of the protein.

A

The final vaccine construct was designed in the following sequential order: (4 HTL L1+ 4 HTL L2) + (4 LBL L1+ 2 LBL L2) + (5 CTL L1+ 6 CTL L2)

MDWTWILFLVAAATRVHSEAAAKAKFVAAWTLKAAAGGGGGGSMDFATLQANKSDVPLGGGGSDNRENVSMDYKQTQLGGGG
SARHFFNRAGTVGEKEGGGGSRENVSMDYKQTQLCIGGGGSADKILQWGSLGVFFGGGGSIADKILQWGSLGVFFGGGGSTSG
FEITSSSTDEATGGGGSDKILQWGSLGVFFGGKKRVRLPDPNKFGLPDTSKKFVTVVDTTRSTNMTLCKKGQPLGVGISGHPLLNK
KKRHVEEYDLQFIFQLCKKTGSGTGGRTGYVPLGTKKGGLGIGTGSGTGGRTGEAAAKYVTRTNIYYEAAAKMVDTGFGAMEAA
AKVEVGRGQPLEAAAKEEYDLQFIFEAAAKWEVDLKEKFEAAAKILQWGSLGVEAAAKRRKRIPYFFEAAAKKRRKRIPYFEAAAK
VRFSRLGQKEAAAKSRLGQKATMEAAAKLQWGSLGVFEAAAKPEVTLRCWALGFYPEEILLTWQRNGEDLTQDMELVETRPSGD
GNFQKWAALGVPSGEEQRYTCRVQHEGLQGPLTLRWEPPQPFVPIMGIIHHHHHH

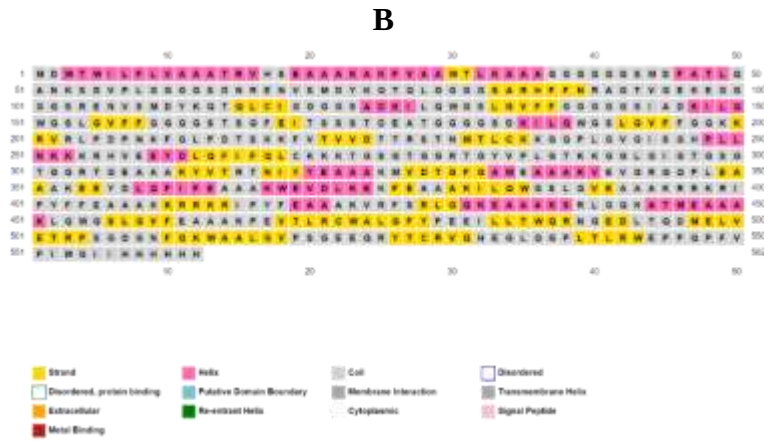

C

```
Sequence length :   562

SOPMA :
   Alpha helix      (Hh) :   129 is  22.95%
   3(10) helix      (Gg) :     0 is   0.00%
   Pi helix         (Ii) :     0 is   0.00%
   Beta bridge      (Bb) :     0 is   0.00%
   Extended strand  (Ee) :   158 is  28.11%
   Beta turn        (Tt) :     0 is   0.00%
   Bend region      (Ss) :     0 is   0.00%
   Random coil      (Cc) :   275 is  48.93%
   Ambiguous states (?)  :     0 is   0.00%
   Other states          :     0 is   0.00%
```

Figure 7. Prediction of secondary structure (2D) of chimeric L1/L2 mRNA-based vaccine. The chimeric L1/L2 mRNA-based vaccine construct's open reading frame amino acid sequence begins with helper T lymphocyte (HTL) epitopes, followed by linear B-cell (LBL) epitopes, and ends with cytotoxic T lymphocyte (CTL) epitopes. Specifically, this vaccine consists of 4 HTL epitopes from L1 and 4 from L2, then 4 LBL epitopes from L1 and 2 from L2, and finally 5 CTL epitopes from L1 and 6 from L2, linked together with the proper linkers (EAAAK, GGGGS, and KK) (**A**). In the open reading frame (ORF) of the vaccine, there is a PADRE sequence that is underlined and an IgESP (immunoglobulin E signal peptide) that is highlighted in yellow at the N-terminal. There is also an MITD sequence that is highlighted in green and an orange 6xHis tag at the C-terminal. The legend within the picture (**B**) explains how the different sections (helixes, strands, coils) are colored. The 2D structure was constructed with PSIPRED (**B**), while conformation states were generated with the NPSA/SOPMA web server (**C**).

Validation and modeling of the vaccine construct's tertiary (3D) structure

The trRosetta server indicated that the overall evaluation of protein quality parameters was high, as determined by PROCHECK (Ramachandran plot analysis) and ProSA online services, after 3D structural refinement. Figure 8B illustrates that the improved model had 96.1%, 3.5%, 0.4%, and 0.2% of the residues situated in the most favored, additional allowed, generously allowed, and forbidden zones, respectively. The refined construct had a Z-score of -7.2, signifying high quality ($Z < 0$; Figure 8C), and an ERRAT quality factor of 88.3721. The ERRAT server was employed to analyze the non-bonded interaction data. The GalayxRefine2 website indicated that the refined 3D structure exhibited GDT-HA scores of 0.9644, a root mean square deviation (RMSD) of 0.372, a MolProbity score of 1.390, a clash score of 7.1, poor rotamers at 0.2, and a Ramachandran preferred score of 98.8. This finding suggests that the modeled protein demonstrated high stereo-chemical quality, with the majority of its residues occupying energetically favorable conformations.

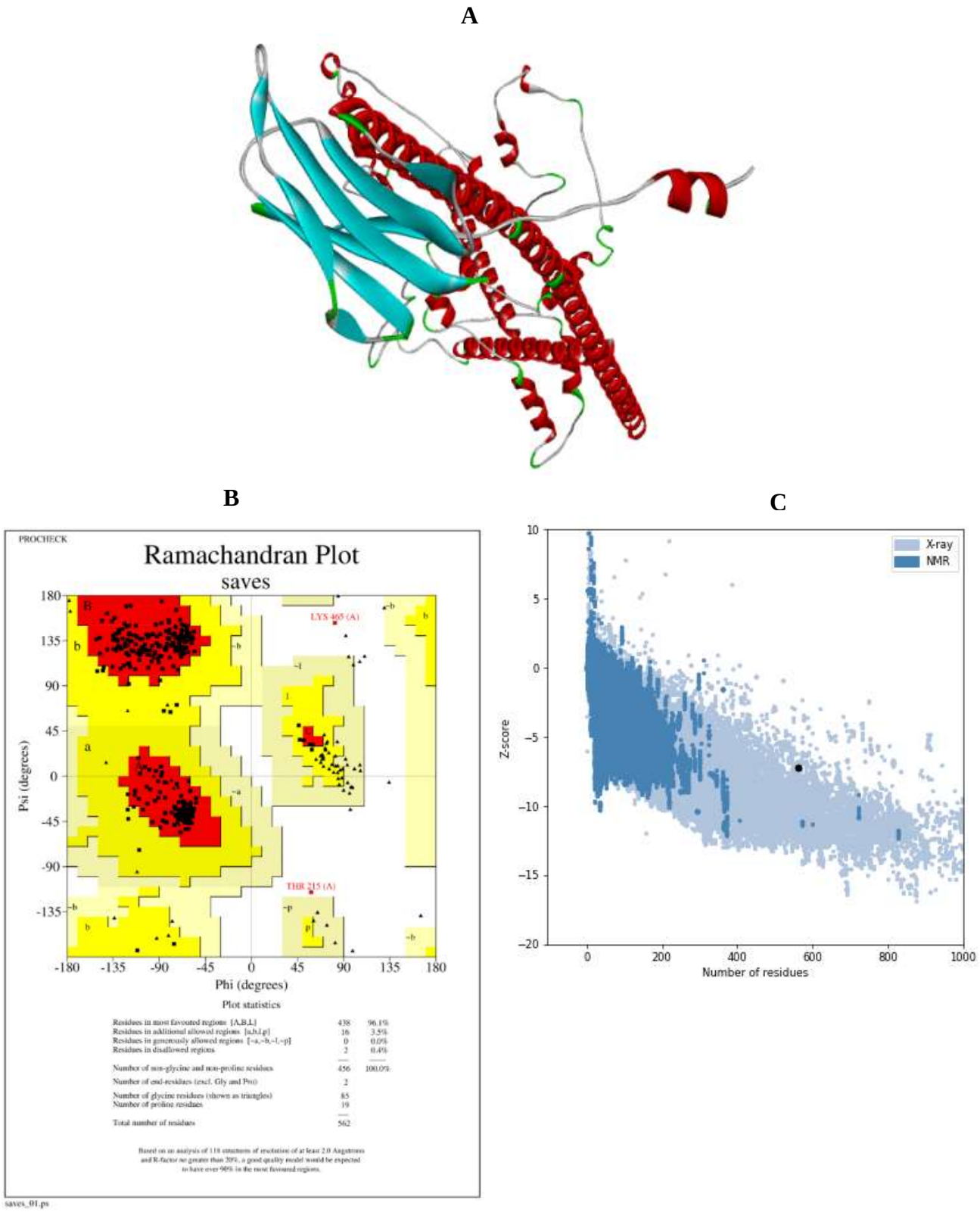

Figure 8. Validation of the vaccine design's 3D structure with a Ramachandran plot and the ProSA web server. 3D model of the vaccine (**A**), validation of the model's 3D structure using a Ramachandran plot, with (96.1%) residues in the most preferred region (**B**), and overall model quality with a Z-Score value of (-7.2) using ProSA (**C**).

Identification of non-linear/discontinuous B-cell epitopes

ElliPro was employed to identify non-linear B-cell epitopes on the vaccine's 3D structure, using a threshold of a minimum score exceeding 0.5 and a maximum distance of 6 angstroms (6 Å) as the default parameters. The findings revealed that the formulated vaccine contained numerous non-linear B cell epitopes within its three-dimensional structure (Figure 9 and Table 6).

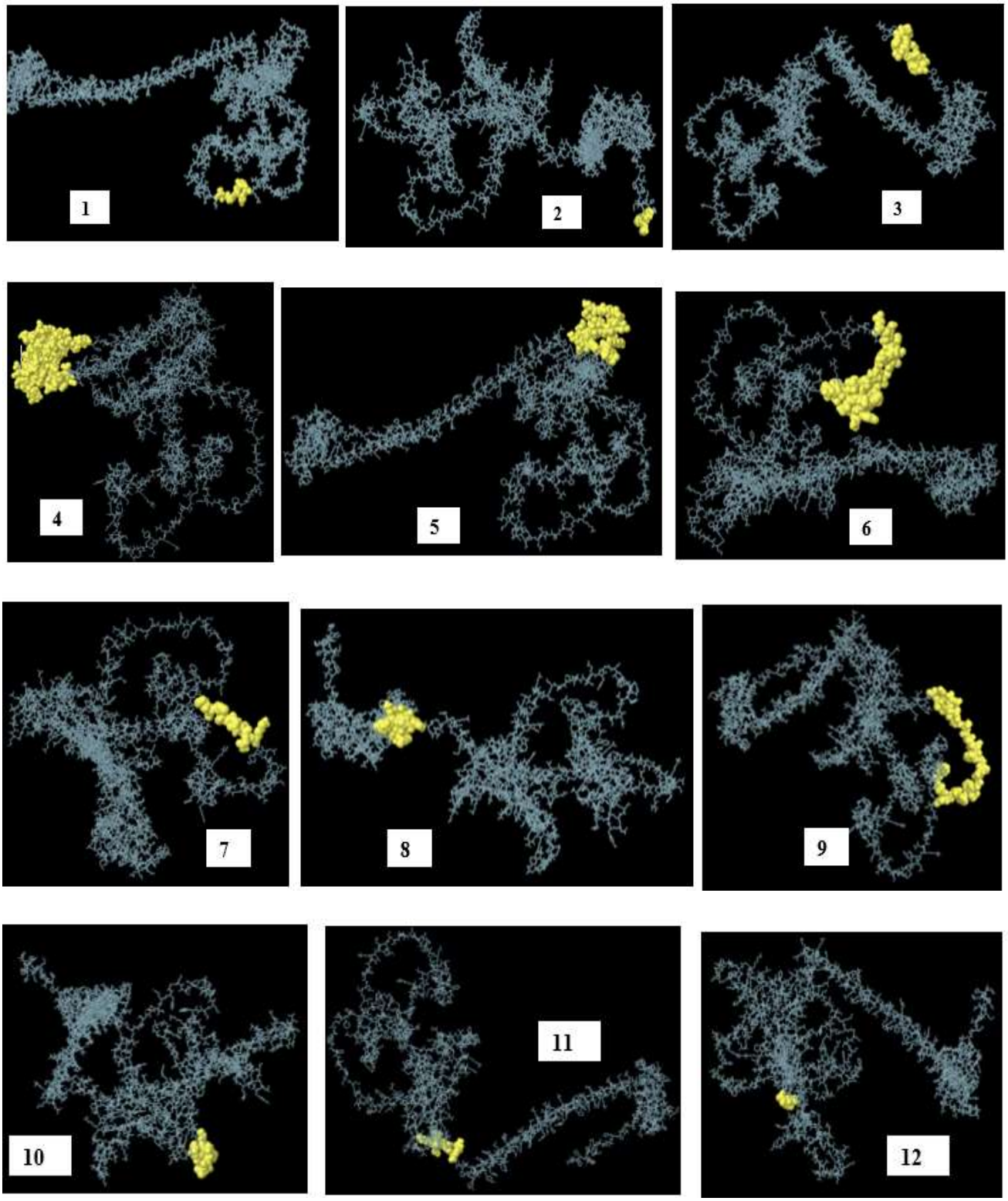

Figure 9. Discontinuous B cell epitopes in the chimeric L1/L2 mRNA-based vaccine 3D structure (1-12). The vaccine design is shown by gray sticks, whereas cyan spheres depict the discontinuous B cell epitopes. The numbers (1-12) demonstrate residues and their corresponding scores as shown in Table 6.

Table 6. List of predicted conformational /discontinuous B-Cell epitopes in the final vaccine construct

No.	Residues	Number of residues	Score
1	A:N106, A:V107, A:S108, A:M109, A:D110, A:Y111	6	0.979
2	A:H560, A:H561, A:H562	3	0.969
3	A:F549, A:V550, A:P551, A:I552, A:M553, A:G554, A:I555, A:I556, A:H557, A:H558, A:H559	11	0.895
4	A:S438, A:R439, A:L440, A:G441, A:Q442, A:K443, A:A444, A:T445, A:M446, A:E447, A:A448, A:A449, A:A450, A:K451, A:L452, A:Q453, A:W454, A:G455, A:S456, A:L457, A:G458, A:V459, A:F460, A:E461, A:A462, A:A463, A:A464, A:K465, A:P466, A:E467, A:V468, A:T469, A:L470, A:R471, A:C472, A:W473, A:A474, A:L475, A:G476, A:F477, A:Y478, A:P479, A:E480, A:E481, A:I482, A:L483, A:L484, A:T485, A:W486, A:Q487, A:R488, A:N489, A:G490, A:E491, A:D492, A:L493, A:T494, A:Q495, A:D496, A:M497, A:E498, A:L499, A:V500, A:E501, A:T502, A:R503, A:P504, A:S505, A:G506, A:D507, A:G508, A:N509, A:F510, A:Q511, A:K512, A:W513, A:A514, A:A515, A:L516, A:G517, A:V518, A:P519, A:S520, A:G521, A:E522, A:E523, A:Q524, A:R525, A:Y526, A:T527, A:C528, A:R529, A:V530, A:Q531, A:H532, A:E533, A:G534, A:L535, A:Q536, A:G537, A:P538, A:L539, A:T540, A:L541, A:R542, A:W543, A:E544, A:P545, A:P546, A:Q547, A:P548	111	0.776
5	A:T232, A:L233, A:C234, A:K235, A:K236, A:G237, A:Q238, A:P239, A:L240, A:G241, A:V242, A:G243, A:I244, A:S245, A:G246, A:H247, A:P248, A:L249, A:L250, A:N251, A:K252, A:K253, A:K254, A:R255	24	0.741
6	A:D64, A:N65, A:E67, A:N68, A:V69, A:S70, A:M71, A:D72, A:Y73, A:K74, A:Q75, A:T76, A:Q77, A:L78, A:G79, A:G82, A:S83, A:A84, A:H86, A:F87, A:F88, A:N89, A:R90, A:A91, A:G92, A:T93, A:V94, A:G95, A:E96, A:K97, A:G99, A:G100, A:G101, A:G102, A:S103, A:R104, A:E105	37	0.74
7	A:K112, A:Q113, A:T114, A:Q115, A:L116, A:C117, A:I118, A:G119	8	0.724
8	A:G345, A:Q346, A:P347, A:L348, A:E349, A:A350, A:A351, A:A352, A:K353, A:E354, A:E355, A:Y356, A:D357, A:L358, A:Q359, A:F360, A:I361, A:E363, A:A364, A:K367	20	0.701
9	A:W151, A:G152, A:S153, A:L154, A:G155, A:V156, A:F157, A:F158, A:G159, A:G160, A:G161, A:G162, A:S163, A:T164, A:S165, A:G166, A:F167, A:E168, A:I169, A:T170, A:S171, A:S172, A:S173, A:T174, A:D175, A:E176, A:A177, A:T178, A:G179, A:G180, A:G181	31	0.682
10	A:G282, A:Y283, A:V284, A:P285, A:L286, A:G287, A:T288, A:K289, A:G291, A:G292, A:L293, A:G294, A:I295, A:G296	14	0.594
11	A:A338, A:K339, A:V340, A:E341, A:V342, A:G343, A:R344	7	0.528
12	A:A36, A:G37, A:G38, A:G39, A:G40	5	0.511

To cite this paper: Sylvere N, Kimotho J, and Ngugi CW (2025). Immunoinformatics Approach to Develop a Novel Chimeric L1/L2 Messenger RNA-based Vaccine Targeting a Broad Spectrum of Human Papillomavirus Species. *World Vet. J.,* 15(2): 341-374. DOI: https://dx.doi.org/10.54203/scil.2025.wvj37

Molecular docking analysis

To determine the modes and energies of the proposed vaccine against human TLR4 and TLR9, molecular docking techniques were applied. The ClusPro 2.0 server produced the top five ranked models of the docking complex between the vaccine and TLR4. The optimal model, encompassing 52 members, demonstrated the lowest binding energy value of (ΔG = -1377.5 kcal/mol) and was therefore selected for further analysis (Figure 10). This model showed a representative center with a weighted score value of -1363.1. The interactions between residues were resolved by LigPlot+/DIMPLOT (Figure 10II, III, IV). The hydrogen bonds that had formed between residues of vaccine and receptor are: ASN 365 (B): LYS 388 (A); ASN 365 (B): ASN 365 (A); LYS 388 (B): ASN 365 (A); GLN 507 (B): GLN 507 (A); ASP 101 (C): ARG 764 (A); ASP 101 (C): SER 317 (A); TYR 102 (C): ARG 764 (A); SER 103 (C): ASN 266 (A); THR 116 (C):ASN 265 (A); GLN 111 (C):HIS 159 (A); THR 112 (C): GLU 135 (A); THR 112 (C): ARG 87 (A); GLY 110 (C): ARG 87 (A); ARG 68 (C):GLU 42 (A); LYS 109 (C):SER 62 (A); ASP 100 (C): ARG 234 (A); ASP 99 (C): ARG 289 (A); ARG 106 (C): SER 18(A); ARG 106 (C): SER 183 (A); ARG 90 (D): GLU 439 (A); GLY 123 (D): SER 416 (A); LYS125 (D): SER 445 (A); LYS 125 (D): ASN 417 (A); LYS 125 (D): GLU 422 (A).

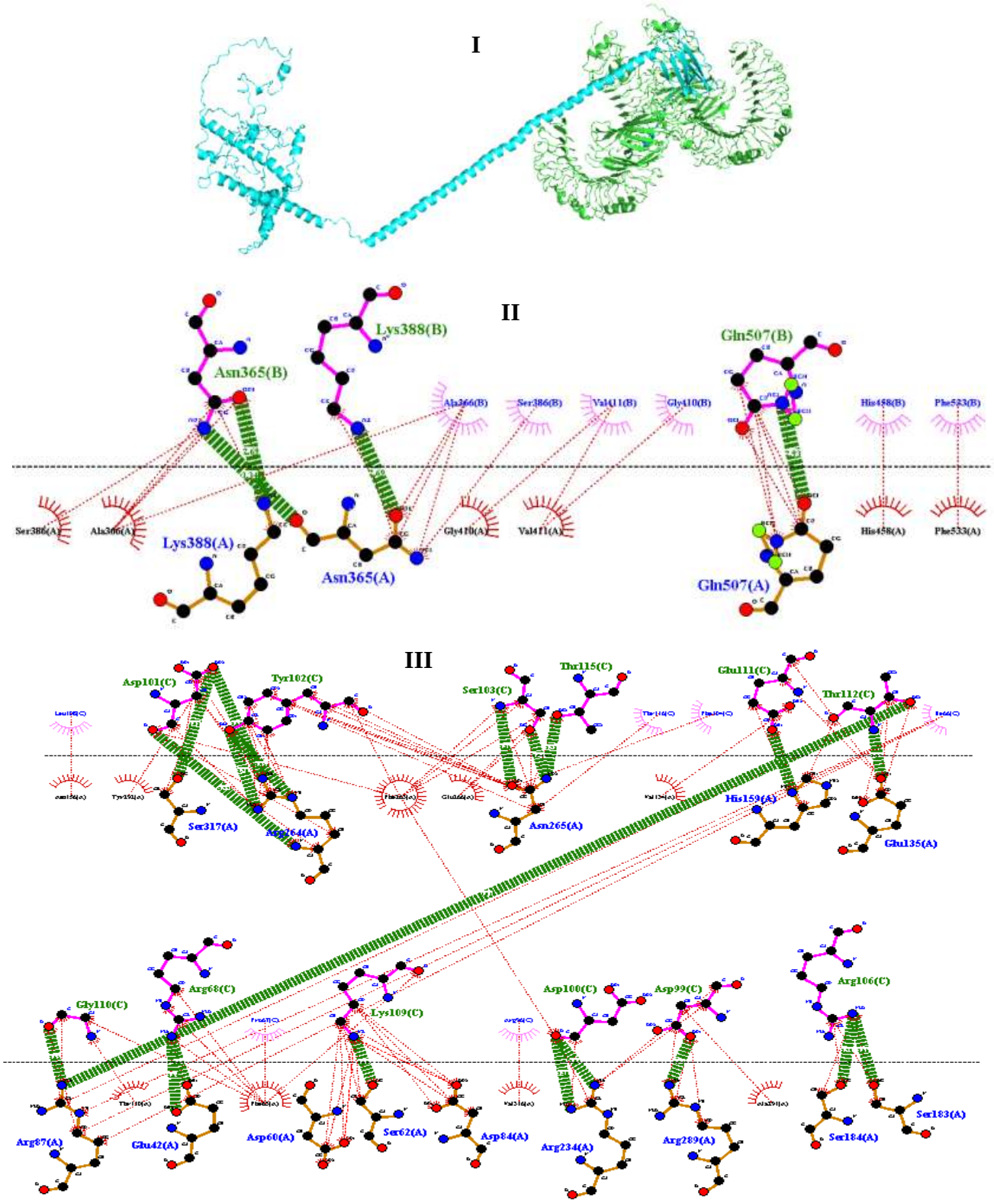

To cite this paper: Sylvere N, Kimotho J, and Ngugi CW (2025). Immunoinformatics Approach to Develop a Novel Chimeric L1/L2 Messenger RNA-based Vaccine Targeting a Broad Spectrum of Human Papillomavirus Species. *World Vet. J.*, 15(2): 341-374. DOI: https://dx.doi.org/10.54203/scil.2025.wvj37

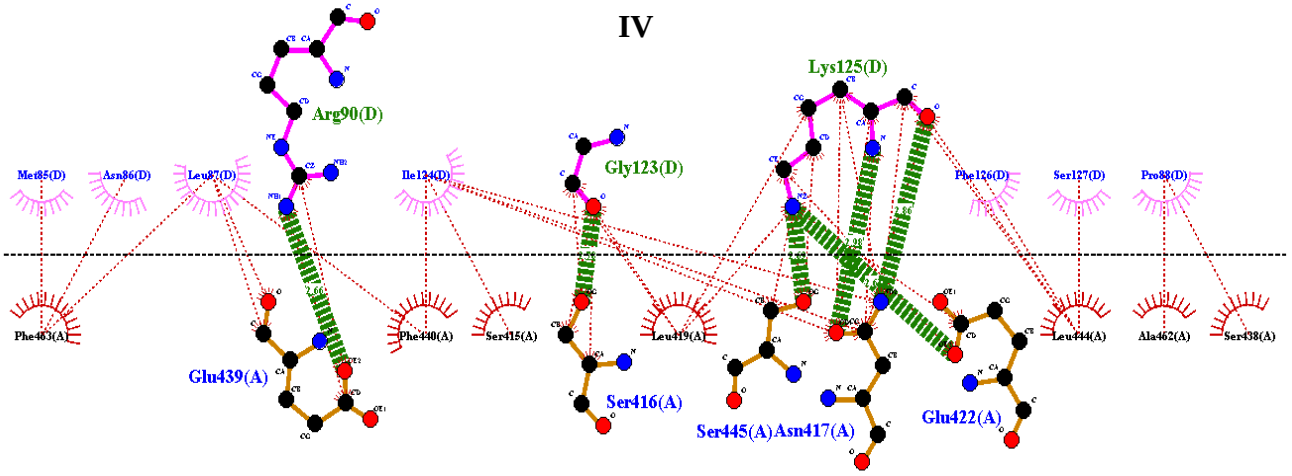

Figure 10. The docked complex between the vaccine and human Toll-like receptor 4 (TLR4) and residue interactions analysis. Docked complex between vaccine and TLR4 (**I**) and its interactions (**II, III, IV**). The vaccine is shown in gray, whereas the receptor is shown in green (**I**). The LIGPLOT+/DIMPLOT displays hydrogen bonds depicted by dashed (green) lines with the bond length displayed inside, while red dashed lines denote hydrophobic interactions.

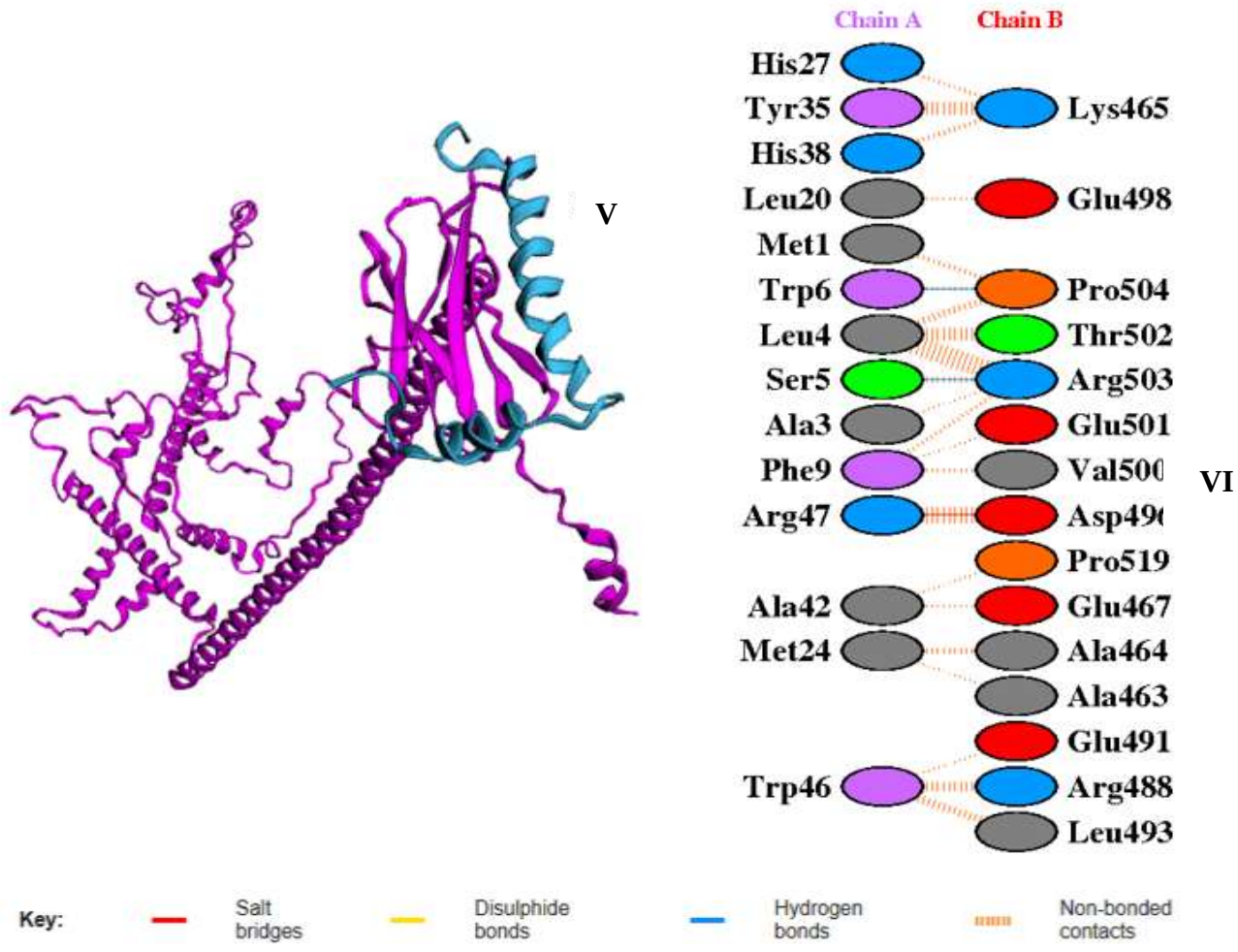

Figure 11. The docked complex between the vaccine and human Toll-like receptor 9 (TLR9) and residue interactions analysis. Schematic diagram of the docking complex between vaccine chain A and TLR9 chain B (**V**), along with their interaction residues (**VI**). The vaccine is highlighted in purple, and TLR9 in blue (**V**). Blue dashed lines represent hydrogen bonds, while salt bridges are shown as red dashed lines (**VI**).

The docking of HLA alleles (MHC-I/II) and B cell receptor with the vaccine was determined using HawkDock Server v2 (Table 7). Docking results indicated that the vaccine interacted effectively with HLA (MHC-I) (PDB ID: 6TDS, HLA-A02:01), scoring -4772.84 and having a binding free energy of (ΔG = -34.01 kcal/mol). The docking analysis of the vaccine against HLA (MHC-II) (PDB ID: 1BX2, HLA-DR2, DRA*0101) yielded a score of -5281.54 and a binding free energy of (ΔG = -20.77 kcal/mol). Finally, the vaccine-BCR interaction resulted in a score of -4004.84 and a binding free energy of (ΔG = -34.41 kcal/mol).

Table 7. Docking analysis between vaccine and B-cell receptor, human leucocyte antigen, and Toll-like receptors 4 and 9

Receptors	Alleles PDB ID	Binding free energy (ΔG kcal/mol)	Score of top-ranked models
Vaccine-BCR	PDB ID: 3KG5	-34.41	-4004.84
Vaccine- MHC class I	CTL (PDB ID: 6TDS, HLA-A02:01)	-34.01	-4772.84
Vaccine- MHC class II	HTL (PDB ID: 1BX2, HLA-DR2, DRA*0101)	-20.77	-5281.54
Vaccine-TLR4	(PDB ID: 3FXI)	-1377.5	-1363.1
Vaccine-TLR9	(PDB ID: 8AR3)	-24.19	-3015.32

BCRs: B-cell receptors, HLA: Human leucocyte antigen, MHC-I/II: Major histocompatibility complex class I and II, TLR4 and TLR9: Toll-like receptors (4 and 9), PDB: Protein data bank, HTLs: Helper T lymphocytes

Molecular dynamics simulation

Molecular dynamics simulation (iMODs) changes the complex's force field over time to do structural critical analysis. Figure 12 illustrates the molecular dynamics simulation results of interatomic interactions between the vaccine and Toll-like receptors. The iMODs results for the vaccine-TLR9 complex (Figure 12A) showed an increase in deformability (Figure 12B). The NMA profile is more flexible than the PDB profile, as shown by the B-factor (Figure 12C), variance (%) (Figure 12D), eigenvalues with a minimum Eigenvalue of 2.735661e-05 (Figure 12E), a covariance map depicting correlated (red), uncorrelated (white), and anti-correlated (blue) motions of paired residues (Figure 12F), and the elastic network (Figure 12G).

The interaction between the vaccine and TLR4 (Figure 12H) exhibited protein deformability or variations at each residue capacity level (Figure 12I). This was due to the complex possessing regions with varying elevations, including lower and higher hinges or peaks. The ligand-receptor combination remained stable in dynamic conditions, as indicated by the RMSD plot, which showed lower deformability. These findings collectively indicated that stable RMSD plots and low deformability in molecular dynamics simulations serve as indicators of structurally stable vaccine constructs, which are essential for effective immune recognition and vaccine efficacy.

Figure 12J shows the complex's NMA and PDB fields, along with a B-factor that indicated the degree to which atoms or residues in a molecule deviate from their normal positions during simulation. The NMA and PDB fields' results revealed a few disordered regions with larger B-factors, corresponding to increased atomic displacement, indicating flexible loops that enhance antigen presentation and immune recognition. Furthermore, the vaccine-TLR4 compound displayed an Eigenvalue of 5.599239e-08 (Figure 12L). The eigenvalue for each normal mode signifies the rigidity (compactness) of the motion. The covariance matrix or heat map illustrates the correlation of motions between pairs of residues, such as correlated (red), uncorrelated (white), or anti-correlated (blue) behaviors (Figure 12M).

The elastic network model (Figure 12N) illustrates the connections between pairs of atoms through springs, representing interactions among residues, where each dot on the graph signifies a spring linking the corresponding atoms. Dots are color-coded based on stiffness, with darker shades of gray indicating greater stiffness in the springs and lighter shades indicating less stiffness. Overall, the iMODS analysis demonstrated that the vaccine-receptor complexes remained stable and flexible, with regions exhibiting compactness and deformability within the complex's coordinate system.

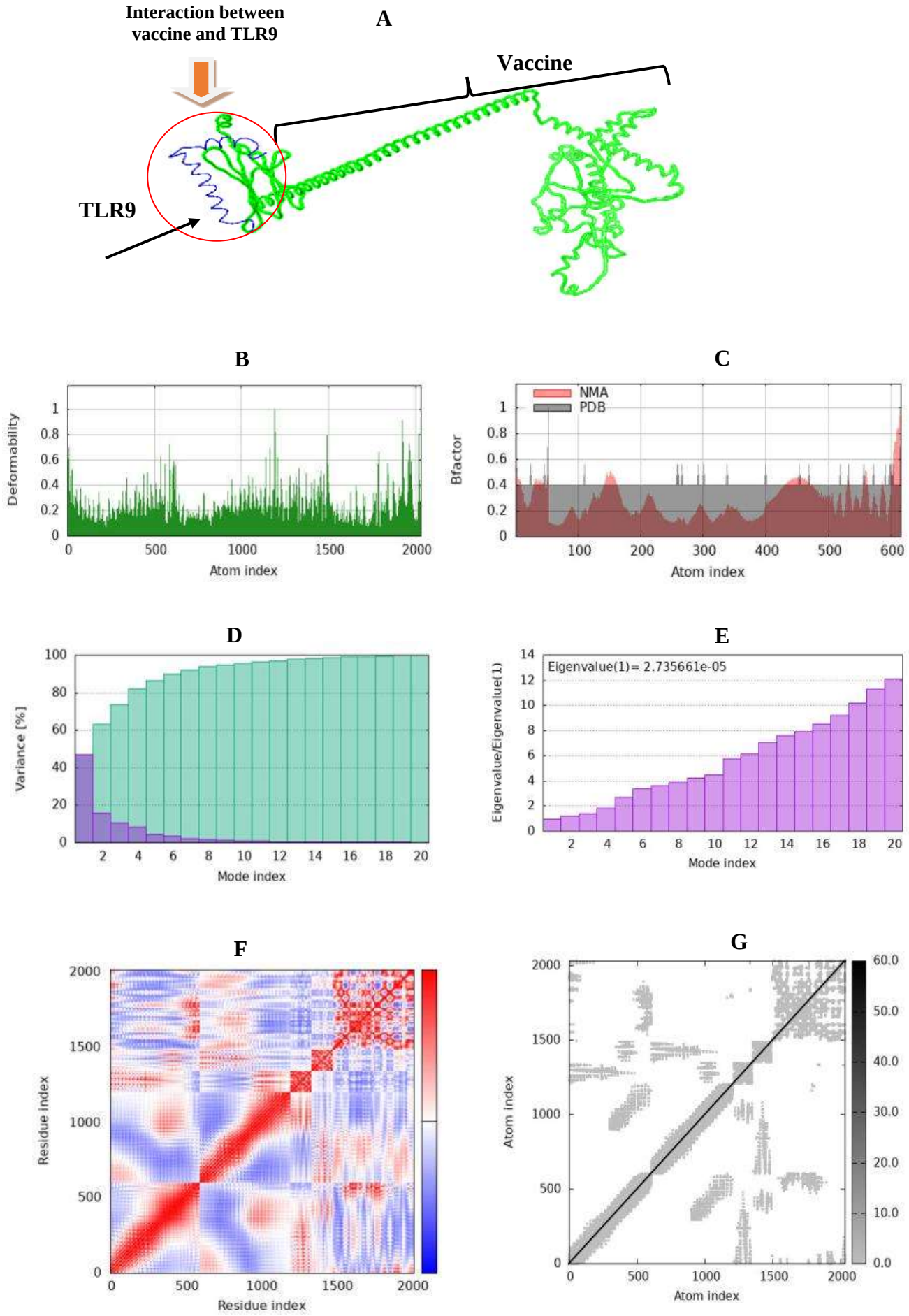
Interaction between vaccine and TLR9
A
Vaccine
TLR9
B
Deformability
Atom index
C
NMA
PDB
Bfactor
Atom index
D
Variance [%]
Mode index
E
Eigenvalue(1)= 2.735661e-05
Eigenvalue/Eigenvalue(1)
Mode index
F
Residue index
Residue index
G
Atom index
Atom index

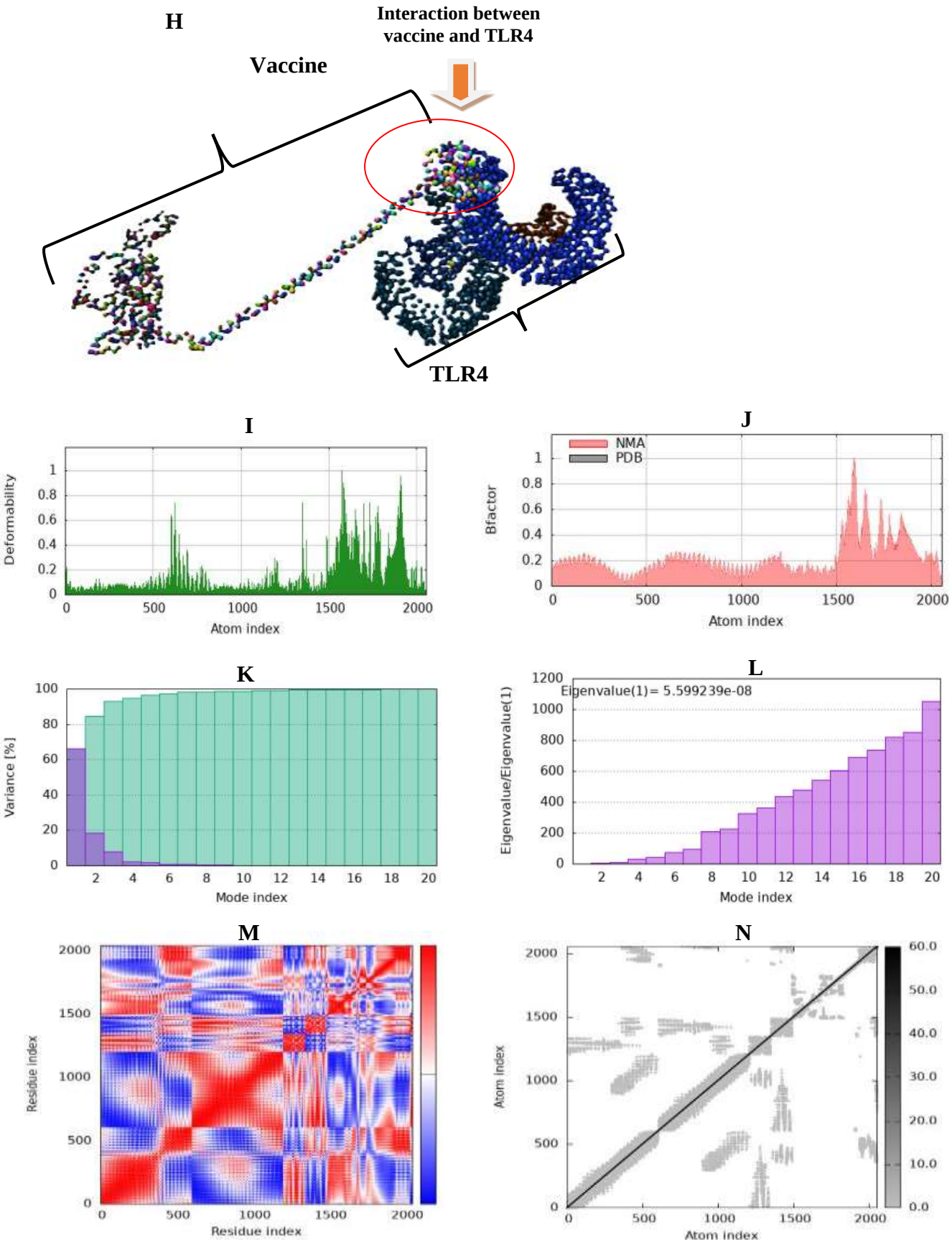

Figure 12. Molecular dynamics simulation analysis of the vaccine design and the docked complexes. The vaccine-TLR9 complex in its NMA mobility, as visualized in the UCSF Chimaera v1.17.3 program (A). **A**: The vaccine is represented in green, while the receptor (TLR9) is highlighted in blue. **B**: The deformability map, **C**: The normal mode analysis (NMA), **D**: Variance (%), **E**: Eigenvalues of 2.735661e-05, **F**: A heat map illustrating the correlated (red), uncorrelated (white), and anti-correlated (blue) movements of paired residues, **G**: An elastic network depicting the connections between atom pairs via springs. **H**: The structure of the vaccine-TLR4 complex, **I**: Deformability vaccine-TLR4 complex, **J**: The correlation between its NMA and PDB fields, and a B-factor, **K**: Variance (%), **L**: Eigenvalues 5.599239e -08, **M**: Covariance map illustrating correlated (red), uncorrelated (white), and anti-correlated (blue) motions of paired residues (M), **N**: Elastic network.

Immune simulation of the multi-epitope chimeric vaccine

The C-IMMSIM tool simulates the binding of B-cell epitopes, class I and II HLA epitopes, and T-cell receptors to HLA peptide complexes. Figure 13A illustrates that the antigen count experienced a steep increase with a peak antigen count of ~650,000 Ag/mL at day 14-15, indicating the introduction of the antigen, followed by a quick fall at day 16, and signifying effective immune clearance. Minor secondary peaks indicated potential booster effects or numerous antigen administrations.

The IgM response began increasing around day 10 and reached its peak at approximately day 18 (90,000 arbitrary units), a typical pattern for a primary immune response, followed by a rapid decline after day 25. This can be seen in Figure 13A, which showed both primary and secondary antibody responses. The IgG response, including IgG1, IgG2, and combined IgG, increased sharply after the antigen peak, indicating a strong adaptive memory response from the immune system. An extensive presence of IgG1 and IgG2 was found, beginning to increase around day 15 and reaching a peak of roughly 100,000 arbitrary units around day 30, with IgG1 predominating, indicating a T-helper (Th2)-biased humoral response. The combined IgM and IgG responses peaked at approximately day 20, reaching around 110,000 arbitrary units, and maintained a high level until the end of the simulation at approximately day 35. The elevated total Ig response indicates enduring immunity.

The immunological simulation results in Figure 13B demonstrated B cell dynamics after vaccination. The total B cell population remained stable until day 10, then experienced a significant increase around day 15, signifying a time of immunological activation. The plateau following antigen clearance indicates the establishment of memory. A decline in naive (non-memory) B cells was observed around day 15, as they transformed into activated B cells and memory B cells. Memory B cells proliferated rapidly, stabilizing at ~350 cells/mm³ when exposed to antigens, and then entered a stable phase, indicating long-term immunity. The existence of permanent memory B cells signifies a strong adaptive response. Furthermore, the designed vaccine induced the production of B cells antibody isotypes, including B Isotype IgM, B Isotype IgG1, and B Isotype IgG2 (Figure 13B). IgM peaked early (on day 15), with a count of ~500 cells/mm³, which shows a primary immune response. Conversely, IgG1 significantly surpassed IgG2 on day 15, stabilizing at around 100 cells/mm³ and 50 cells/mm³, respectively, after IgM, indicating class switching and the initiation of long-term immunity. The fact that IgG1 was more common than IgG2 shows a Th2-skewed response, which is typical of protein subunit vaccines and some mRNA vaccines.

The immune simulation results of the vaccine presented in Figures 13CDF suggested that the immune system was activated approximately 35 days post-vaccination. These results showed important responses from the macrophage (MA), dendritic cell (DC), and T-helper (TH) cell populations. The data showed that the total number of macrophages remained mostly unchanged, cycling between active and resting states (Figure 13C), thereby avoiding excessive immune exhaustion. Around day 15, the internalized antigen and the rise in presenting macrophages reached their peak, which means that antigens are being absorbed and presented to T cells. Another observation was that the active and resting states of macrophages oscillated, indicating ongoing immunological control.

A rapid increase (~days 10–15) in total TH cells indicated a vigorous adaptive immunological response. Additionally, an increased proliferation of total TH cells was noticed, reaching approximately 1,2000 cells/mm³ around days 15 to 20, signifying a robust adaptive immune response. The quantity of memory T-helper cells increased to approximately 1,000 cells/mm³, providing sustained protection. Figure 13F illustrates that the presence of dendritic cells (DCs) escalated around day 15, indicating effective antigen acquisition and T cell activation. The present vaccine induced sustained amounts of resting and active dendritic cells to avert immunological overactivation.

The immunological simulation results demonstrated that the vaccine generated several cytokines, including interferons (IFN), interleukins, and regulatory cytokines (Figure 13E). A significant increase in IFN-γ, peaking approximately ~550,000 ng/µL at day 15, followed by a gradual decline, was observed. IL-2 response peak reached around ~750,000 ng/µL at around day 17, followed by a rapid decline afterward, demonstrating the vaccine‘s capacity to stimulate proliferation and activation of T-cells. Furthermore, the vaccine was shown to stimulate the production of Interleukin-12 (IL-12). This serves as a crucial immunomodulatory molecule in vaccine design by promoting Th1-type immune responses, enhancing cytotoxic T lymphocyte activity, and stimulating interferon-gamma production.

Finally, regulatory cytokine, including IL-10, showed an increase around 40,000 ng/µL at (around day 16), reaching a peak at around day 17. The study observed a significant increase in T-helper cells, including memory T-helper cells, as well as CTL, dendritic cells, and macrophages. Additionally, the vaccine elicited the activity of natural killer cells. These findings suggest that the vaccine candidate induced a robust and effective immune response, potentially protecting against the targeted disease.

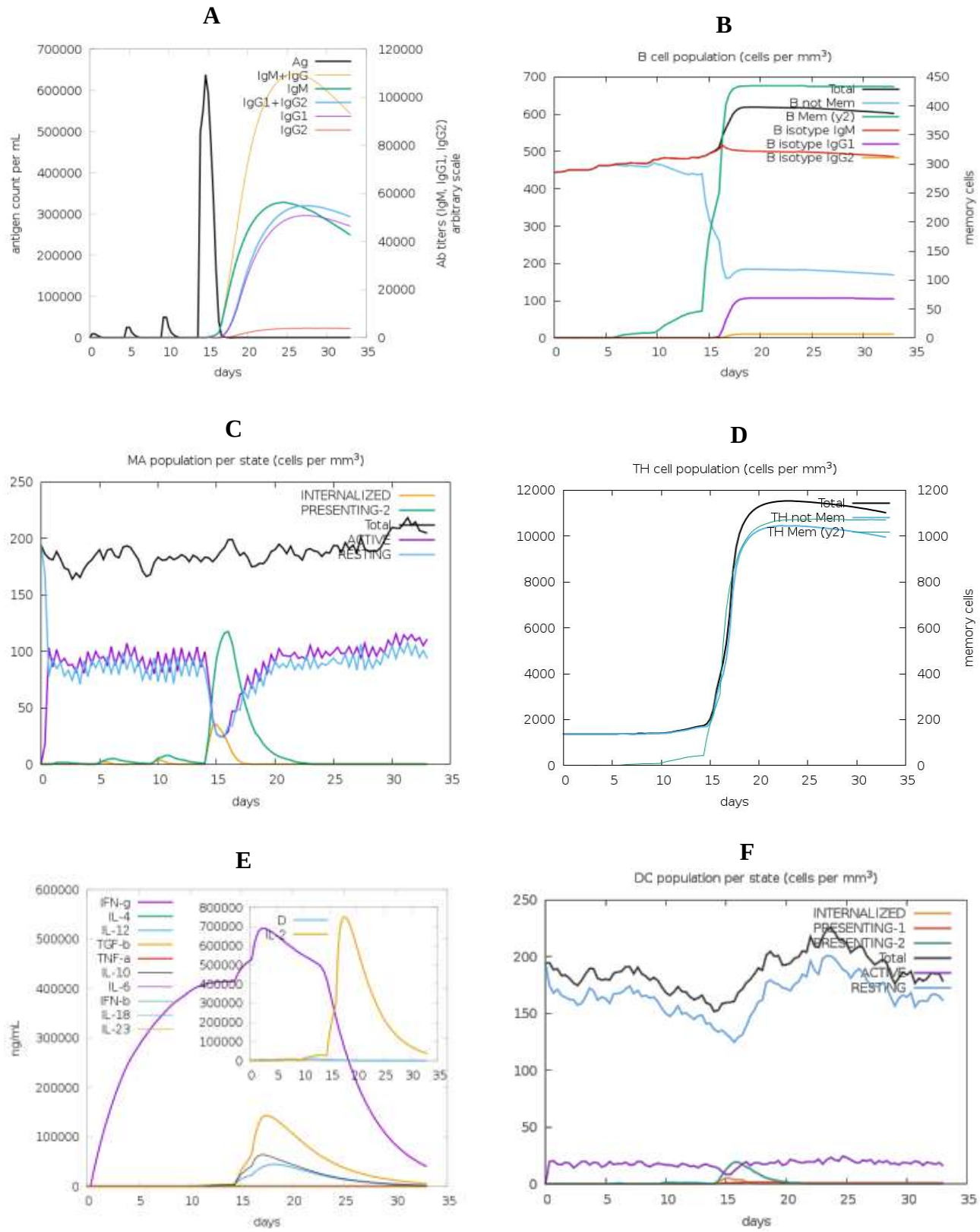

Figure 13. Different immune responses are generated by the C-ImmSim server. **A**: The immunoglobulins produced in response to antigen (Ag) injection are shown in the panel. **B**: B cell population in response to Ag injections, **C**: Macrophage population by state, **D**: Population per state of T-helper cell, **E**: Production of cytokines and interleukins (increased production of IFN-γ, IL-2, IL-10, and IL-12**, F**: DC population by state.

Codon-optimization and *in silico* cloning

The final chimeric vaccine was codon-optimized for *Homo sapiens* using the VectorBuilder online tool. The optimized mRNA open reading frame comprised 1686 nucleotides. The findings indicated that the mRNA sequence of the vaccine exhibited a CAI of 0.91, suggesting stability in the mRNA sequence. The vaccine exhibited a GC content of 59.92%, indicating its potential for efficient expression in human cells. The optimal GC content for effective expression typically ranges from 30% to 70%, while a CAI value above 0.8 is considered acceptable for robust expression in the host organism. Subsequently, the entire mRNA vaccine sequence was inserted into the standard custom cloning vector pUC57 using SnapGene software, between the EcoRI (GAATTC) and SacI (GAGCTC) restriction sites.

Additionally, the BspQI (GCTCTTC) restriction enzyme sequence was added to the constructed vaccine after the poly (A) tail to facilitate plasmid DNA linearization during IVT mRNA synthesis. The resulting plasmid vector construct "chimeric L1/L2_pUC57" consisted of 4725 bp, comprising 2027 bp of the inserted sequence (Figure 14). After that, the entire mRNA vaccine was inserted using SnapGene software between the two restriction sites of EcoRI (GAATTC) and SacI (GAGCTC) in the standard custom cloning vector pUC57. This plasmid is suitable for cloning due to its efficient replication capabilities. GenScript provided the plasmid vector.

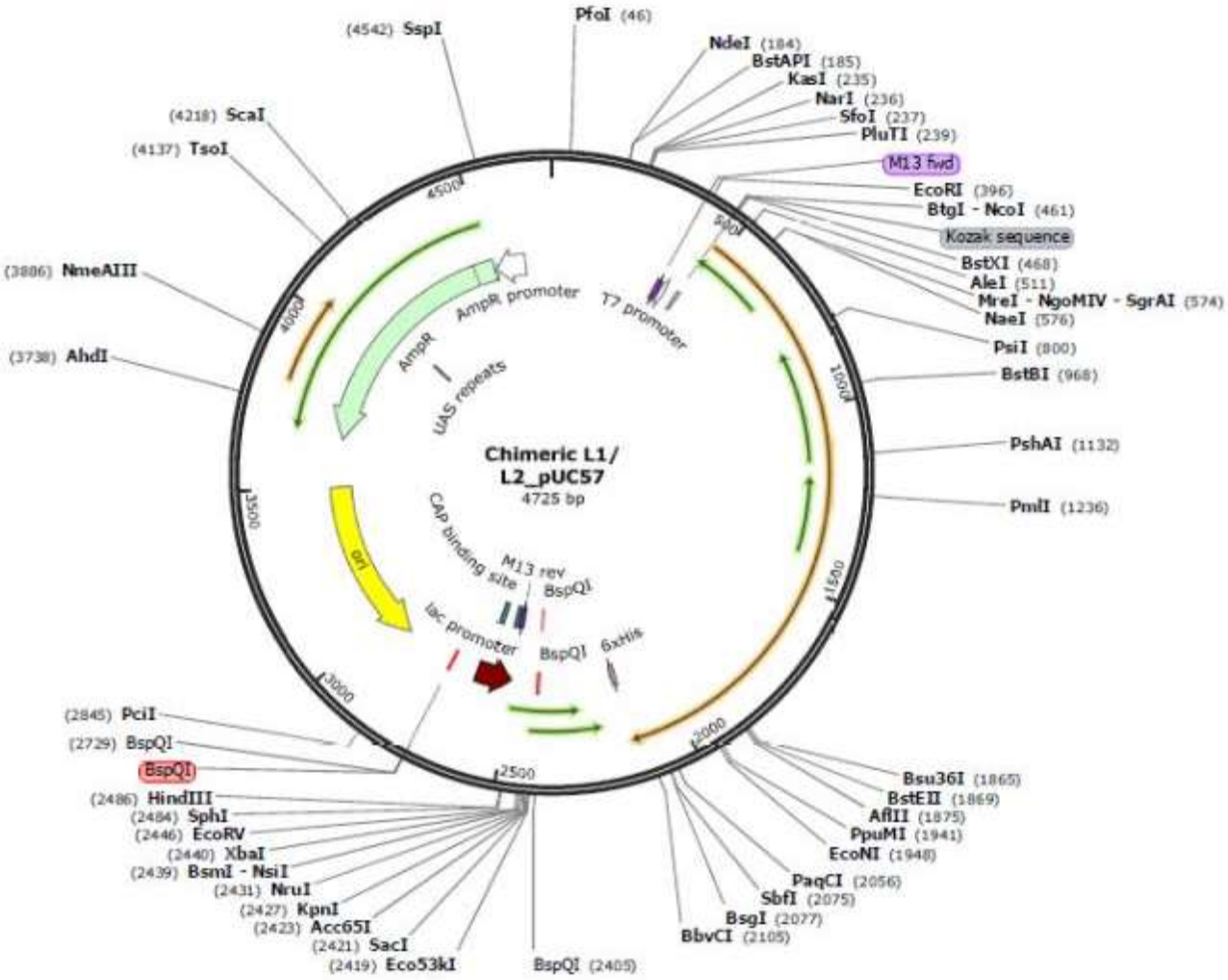

Figure 14. Cloning simulation of the final vaccine construct against human papillomavirus species in the pUC57 standard vector (size of 4725 bp) between the EcoRI (at a position of 396) and SacI (at a position of 2421). The red spots represent (BspQI) restriction sites for plasmid DNA linearization, whereas the longer orange arrow represents a multi-epitope chimeric L1/L2 mRNA vaccine of 2027 bp length.

Assessment of the vaccine mRNA structure

The RNAfold web server was used to calculate the minimum free energy (MFE) of the mRNA vaccine, yielding an MFE of -731.10 kcal/mol. The centroid secondary structure exhibited a value of -527.51 kcal/mol. Furthermore, the thermodynamic ensemble had a free energy of (-757.80 kcal/mol), a frequency of 0.00% for the MFE structure, and an ensemble diversity of 560.43 (Figure 15). These results suggested that following synthesis, the mRNA might be stable. The structure displayed in Figure 15 is colored by base-pairing probabilities. For unpaired regions, the color denotes the probability of being unpaired.

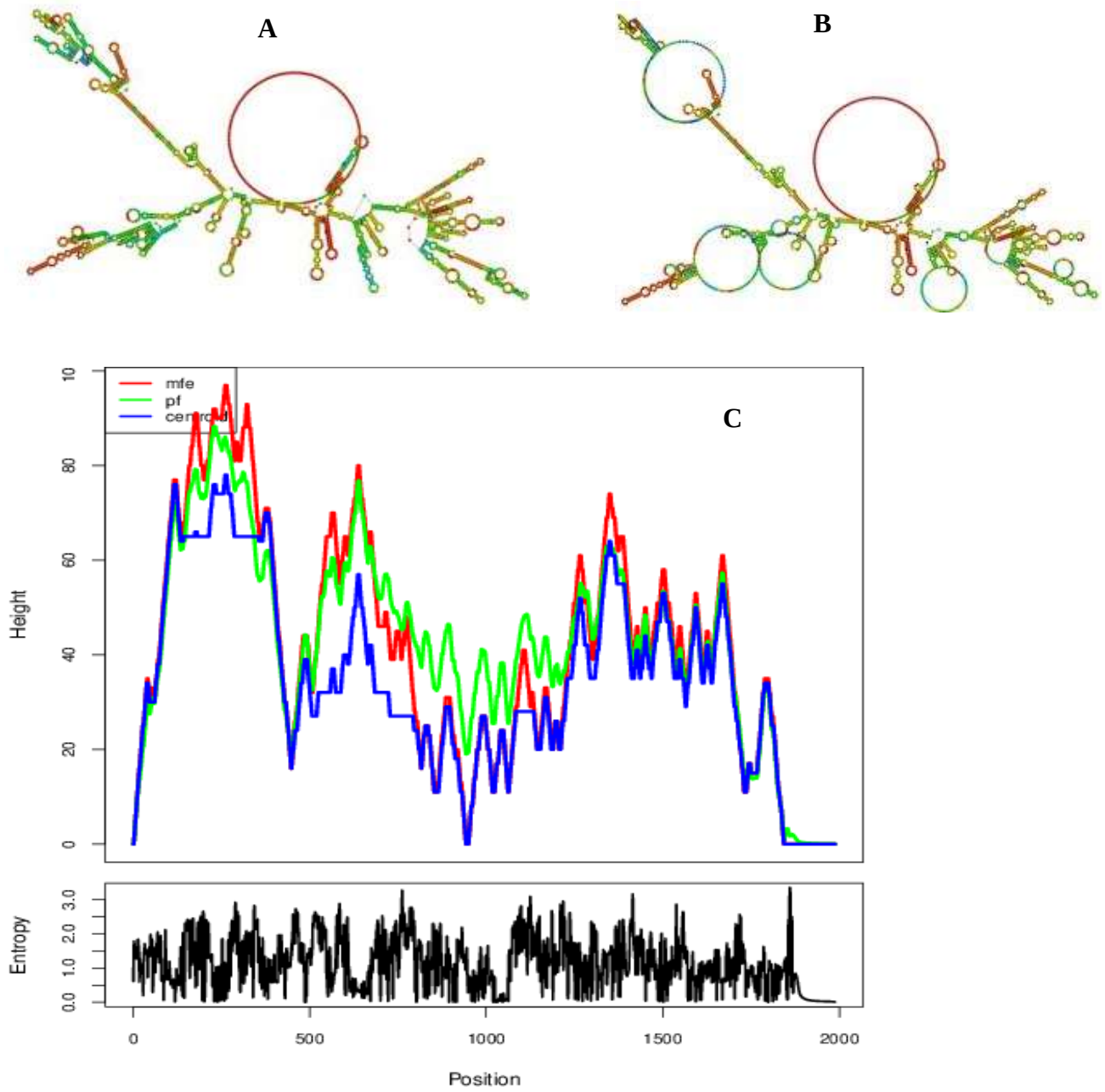

Figure 15. The secondary structure prediction of the final constructed mRNA-based vaccine. **A**: The model of the vaccine's MFE secondary structure. **B**: The predicted model of the vaccine's centroid secondary structure. **C**: A mountain plot illustrating the MFE structure, the thermodynamic group of mRNA structures, the centroid structure, and the positional entropy plot for each nucleotide position. In this plot, red represents MFE, green denotes PF, and blue indicates the centroid.

DISCUSSION

This study developed a chimeric L1/L2 mRNA-based vaccine against different HPVs, a significant health concern that includes cervical cancer (Mahmoudvand et al., 2022). Currently, the US FDA-approved prophylactic vaccines, such as Gardasil-9 and Gardasil-4, which are based on HPV major (L1) capsids, only target a restricted subset of HPV species (Mo et al., 2022). Consequently, they allow untargeted strains to continue spreading infection, highlighting the need for broad protective vaccinations. Developing broad protective vaccinations is a successful strategy to combat the transmission of all kinds of HPV.

Several studies have embraced the development of broad-spectrum vaccinations considering the exploitation of L2 minor capsids due to the underlying highly conserved epitopes across multiple HPV species (Huber et al., 2017; Olczak and Roden, 2020). The L2 capsid, a small protein encoded in HPV genomes, has been studied for its antigenic properties and potential use as a preventive vaccine. Although less immunogenic than the L1 protein, L2 vaccinations stimulate

durable, broad-range immune responses against various HPV infections (Huber et al., 2017; Olczak and Rodent, 2020). A combination of L2 and early viral (L1) antigens may promote both curative and preventive responses (Boxus et al., 2016). The multivalent L2 epitopes (peptide vaccines), fusion or chimeric procedures between L1 and L2, fusion of L1 with other immunogenic proteins, and multi-epitope approaches have emerged as viable options to enhance immunological responses (Namvar et al., 2019).

The creation and development of multi-epitope-based peptide vaccines is an emerging area of research that utilizes specific pathogen components, referred to as epitopes, to formulate vaccinations. The development of epitope-based peptide vaccines is promising due to their relative ease, affordability, rapid design, and protein stability (Shawan et al., 2023). These vaccines can be formulated to target several viral and pathogenic illnesses, including HPV, utilizing multi-epitope peptides (Kumar et al., 2022). Traditional vaccine approaches that effectively prevent numerous diseases encompass live-attenuated, inactivated pathogens, and subunit vaccines; nonetheless, they have yet to meet the criteria for a completely safe, non-allergenic vaccine with rapid development and extensive production capabilities (Mohammadi et al., 2023).

In silico techniques have been used to create peptide vaccines from HPV proteins (Shahab et al., 2023), and prophylactic multi-epitopic DNA vaccines have been developed (Namvar et al., 2019). Plasmid DNA-based vaccines are less preferred due to high costs, complexity, and immunogenicity, along with the potential for anti-DNA antibody production and genomic mutations (Gurunathan et al., 2000), while mRNA vaccines offer low production costs, quick development, and adequate efficacy, making them preferred for preventive and therapeutic applications (Kowalzik et al., 2021).

The use of *in silico* chimeric L1/L2 mRNA vaccine creation is crucial in veterinary medicine, as papillomavirus infections significantly impact both companion animals and humans, resulting in various epithelial lesions and, in some cases, contributing to cancer development (Medeiros-Fonseca et al., 2023). In veterinary medicine, the availability of commercial vaccinations for BPV and COPV is currently limited, often relying on the use of L1 protein-based virus-like particles (VLPs). Nevertheless, these vaccinations may lack extensive cross-protection against different HPV strains. The use of L2 in the chimeric design is anticipated to enhance cross-protection, as L2 encompasses conserved epitopes across multiple HPV types, potentially rendering it a more efficacious strategy for veterinary applications.

Selecting helper T cells (CD4+) and cytotoxic T lymphocytes (CD8+) appears to be a beneficial approach for developing vaccines. This is because cytotoxic T lymphocytes enhance both humoral and cellular immunity, and helper T cells play a crucial role in developing adaptive immune responses. This means that they may play a crucial role in eliminating viruses. The MHC molecules display T cell epitopes that enhance the production of effector cells, immunological memory, and IFN-cells. In this study, the choice of HTLs was based on their capacity to elicit favorable IFN-γ and cytokine responses. Furthermore, linear and discontinuous B-cell epitopes were analysed. The B cell surface membrane receptor contains linear B cells, which are identified by their antigen markers. When a protein adopts its native three-dimensional conformation, it can present conformational (discontinuous) epitopes that are specifically recognized by B cells, leading to the production of targeted antibodies (Lon et al., 2020).

In this study, the best epitopes were joined using the proper linkers, as linkers play a crucial role in epitope presentation, vaccine stability, and overall antigenicity (Tarrahimofrad et al., 2021). The GGGGS linker is very flexible and soluble, which makes it a great choice for fusion protein domains that need to move or interact in certain ways (Chen et al., 2013). The KK linker improves epitope processing and presentation, thereby enhancing immunogenicity. In contrast, EAAAK (a rigid-based linker) enhances immune activation by promoting epitope attachment to adjuvants and providing structural stability across glutamic acid and lysine amino acids (Naveed et al., 2022).

The multi-epitope vaccine construct contained regulatory elements, such as the IgE signal leader peptide, which aids in protein processing and regulates expression, leading to increased immunogenicity (Li et al., 2022). The vaccine construct also included PADRE as an adjuvant or agonist that recruits and activates Toll-like receptors in CD4+ cells (Ghaffari-Nazari et al., 2015). Furthermore, MITD was included in the vaccine due to its role in directing cytotoxic T lymphocyte epitopes to the endoplasmic reticulum compartment (Ghaffari-Nazari et al., 2015; Oladipo et al., 2022). The addition of a polyhistidine tail (6xHis-tag) was incorporated to facilitate protein detection and purification purposes.

The vaccine's chimeric L1/L2 mRNA structure was optimized for efficient human expression, and incorporating untranslated regions (UTRs), Poly (A) tail, and Kozak sequence for maintaining the vaccine's stability, translation efficiency, and immunogenicity (Sun et al., 2023; Jin et al., 2025).

The physicochemical analysis of the designed vaccine revealed an antigenicity score of 0.9178, surpassing the threshold value of 0.4, which suggested a robust ability to provoke immunological responses. The computed solubility was 0.451, which exceeded the average solubility of *E. coli* protein in the experimental solubility dataset (0.45), demonstrating acceptable protein solubility and influencing the efficacy and stability of the vaccine during production and storage. Additionally, the vaccine was found to be non-toxic and non-allergenic, confirming its safety in the body.

The Expasy-ProtParam analysis projected the vaccine to have a molecular weight of 60.16 kDa, with 562 amino acids (aa), indicating an appropriate vaccine candidate. The developed antigenic vaccine demonstrated similar protein properties, as it fell within the allowed range of less than 110 kDa, making it easier to express and purify than larger proteins (Sanami et al., 2023). The molecular weight of a chimeric mRNA-based vaccine was 644.98 kDa, as estimated using the RNA molecular weight calculator online tool. The molecular weight of mRNA-based vaccines can vary significantly depending on their specific design and components, as numerous studies have reported sizes ranging from 285.3 kDa to 71.897 kDa (Naveed et al., 2022; Oladipo et al., 2022). The developed vaccine consisted of multi-epitope peptides with a theoretical pI of 9.44, an aliphatic index of 68.49, and an instability index of 36.89. A protein exhibiting an instability greater than 40 is deemed unstable (Mohammadi et al., 2023). The grand average of hydropathicity (GRAVY) was anticipated to be -0.366, indicating hydrophilicity and its enhanced capacity to interact with neighboring water molecules (Akbay et al., 2021). The predicted half-life of the suggested vaccine design is 30 hours in human reticulocytes, over 20 hours in yeast, and beyond 10 hours in *E. coli*, indicating prolonged stability when interacting with the immune system. The designed vaccine showed comparable physiochemical characteristics, such as high antigenicity potency, protein solubility and stability, hydrophilicity in nature (GRAVY), extended half-life, and accepted molecular weight, as well as the absence of allergens and toxins (MEVs; Ghorban Hosseini et al., 2017; Mahmoodi et al., 2023; Rizarullah et al., 2024). These findings revealed that the produced vaccine is a promising contender for future use, as its physicochemical properties align with those of previous investigations.

The global distribution of HLA alleles, class I and II, necessitates a focus on population coverage when developing effective vaccines to reach the maximum number of people (Shawan et al., 2023). This vaccine achieved a global coverage rate of 86.24%, based on population coverage of T-cell epitopes, as sourced from the IEDB website. Compared to prior and recent prophylactic vaccines, the coverage of the selected T-cell epitopes is inferior to that of the Gardasil-9 vaccine (89.72%); however, it surpassed the finding reported by Ryan et al. (2024) (82.63%). This variability is contingent upon the selected allele, which significantly affects epitope presentation and the predicted efficacy of vaccines across diverse populations (Cai et al., 2021).

The vaccine's 2D structure model identified stable, flexible, and globular secondary structural features in α-helices, β-sheets, turns, and coils. The probability that SOPMA servers will accurately predict the fraction of 2D configurations using four conformational states, alpha helix, sheet, turn, and random coil, is 80% (Hasan et al., 2024). Three-dimensional structural modeling demonstrated that the vaccine included the highest number of amino acid residues in the most favored area, achieving a coverage of 96.1% and a Z-score of -7.2, signifying high quality ($Z < 0$). A high-resolution protein model is expected to have more than 90% of its amino acid residues located within the most favored regions of the Ramachandran plot, indicating robust stereochemical quality (Morris et al., 1992). Additionally, a more negative Z-score reflects better overall structural quality and model reliability (Wiederstein and Sippl, 2007). These attributes significantly reflect the vaccine's stability, transportability, and immunogenicity. The MDockPeP server was used to predict the binding interaction between cytotoxic T cell epitopes and Major histocompatibility class I or HLA alleles. All epitopes, including 5 CTL L1 and 6 CTL2, exhibited an enhanced binding affinity to MHC-I, with a negative free binding energy, indicating a thermodynamically favorable interaction.

In the present study, molecular docking was used to examine how the designed chimeric L1/L2 mRNA vaccine parts interact with HLA alleles, human TLR9 and TLR4, and B cell receptors (BCRs), while molecular dynamics (MD) simulations were used to analyze the stability, flexibility, and behavior of the complex. The vaccine exhibited effective binding affinity with HLA class I, displaying a free energy value of $\Delta G = -34.01$ kcal/mol, and with HLA class II, which showed a free energy value of $\Delta G = -20.77$ kcal/mol. This suggests that the vaccine contains antigenic peptides which immune cells (T cells or B cells) recognize via HLA, resulting in robust cellular and humoral immune responses. The results are corroborated by the findings of Lee et al. (2024), who demonstrated that the HLA-restricted peptide vaccine elicited both T and B cell immunity. Moreover, a significant affinity was observed between the vaccine and TLR4 and TLR9, as well as the B cell receptor (BCR), characterized by the lowest free energy (ΔG). Lower binding-free energy (ΔG) values indicate a more favorable interaction, implying that the vaccine exhibited a vigorous affinity for the receptors. This suggests that the vaccine contained antigenic peptides that trigger robust immune responses in immune cells such as T cells or B cells (Lee et al., 2024). TLR9 plays a critical role in cytokine production and the activation of antigen-presenting cells by recognizing unmethylated CpG motifs commonly found in bacterial and viral DNA (Rottembourg et al., 2010).

The docking analysis results indicated that the vaccine interacted efficiently with receptors, creating hydrogen bonds, salt bridges, and hydrophobic interactions. Crucially, this vaccine should integrate with or be recognized by TLR9 and TLR4. As reported by Lampe et al. (2020), a vaccine that can interact with or be recognized by Toll-like receptors TLR9 and TLR4 is likely to enhance immune activation and exhibit synergistic effects on antigen-presenting cells (APCs), as well as improve the modulation of both innate and adaptive immune responses.

The iMODs were used for Molecular Dynamics simulation to analyze the vaccine-TLR9 and TLR4 complex's stability, flexibility, and functional dynamics. In the present study, normal mode analysis (NMA) was conducted using iMODs to evaluate the stability and dynamic behavior of the designed vaccine in complex with Toll-like receptor TLR9 and TLR4. The deformability plot showed that the vaccine construct had both rigid and flexible parts, with higher deformability observed for the vaccine-TLR 9 complex. Rigidity and flexibility are necessary to maintain the structure's strength and allow the antigen to be presented effectively (Ward and Wilson, 2020). Regions corresponding to predicted epitopes exhibited higher flexibility, suggesting an ability to interact dynamically with immune receptors. Conversely, the core structural elements in TLR4 showed rigidity, ensuring that the construct remains intact upon receptor binding.

The B-factor analysis showed notable variations in the number of atoms located in surface-exposed areas, suggesting that the epitopes are readily accessible. In vaccine design, regions with higher B-factor values generally indicate increased flexibility and surface exposure, making them more likely to be recognized by the immune system (Ullah et al., 2022). Such regions are typically more accessible to antibodies and immune receptors (Soltan et al., 2021).

The elastic network model demonstrated that the vaccine structure maintained a balanced network of interactions between residues, preventing it from becoming too unstable while still allowing it to change its shape. It is known that eigenvalues derived from normal mode analysis (NMA) reflect molecular flexibility and stability (Guan et al., 2025). The vaccine-TLR9 and TLR4 complexes exhibited lower values of eigenvalues, with the vaccine-TLR9 complex demonstrating a lower eigenvalue. The low eigenvalue identified in this study suggested that both vaccine-TLR9 and TLR4 complexes exhibited structural adaptability, facilitating successful receptor binding. A smaller eigenvalue corresponds to a softer mode and a simpler deformation, signifying greater flexibility. Overall, docking and molecular dynamics studies demonstrated that the complexes remain stable during the simulation.

The immunological simulation profile results indicated that the vaccine had exceptional efficacy when administered four times, biweekly, over a 42-day period. This vaccine stimulated the production of B-cells, Helper T Lymphocytes (HTL), Cytotoxic T Lymphocytes (CTL), Natural Killer (NK) cells, macrophages, and the release of interferon (IFN). Interferons and natural killer cells have been documented as primary defenses against invading viruses, including HPV, underscoring their critical role in viral elimination (Shahab et al., 2023). T cells and cytokines are vital in eradicating virus-infected cells (Akbay et al., 2021). The current vaccine corresponds with mRNA vaccines (e.g., BNT162b2, mRNA-1273), which have previously demonstrated a robust IgG-dominant response and rapid antigen clearance (Polack et al., 2020; Baden et al., 2021). In comparison, the current simulation also exhibited a considerable IgG response, indicating effective memory formation. The IgM immune response result indicated that IgM reached its peak early, approximately between days 15 and 17, signifying a typical primary immunological response. Nevertheless, IgM titers subsequently diminished, indicating early activation. Likewise, research on protein subunit vaccinations (e.g., Novavax NVX-CoV2373) generally produced elevated IgG levels, but a delayed IgM response (Heath et al., 2021).

The current vaccine induced a prolonged presence IgG1 and IgG2 responses, with IgG1 dominating, suggesting a Th2-biased humoral response. The current vaccine appeared to induce a more biased immune response toward IgG1, suggesting a heightened Th2 response (humoral immunity, B-cell activation), which may be advantageous for preventing severe disease. Comparably, the COVID-19 vaccine BNT162b2 has been shown to induce human antibody and T (H) 1 T cell responses (Sahin et al., 2021). The elevated IgG levels observed at day 35 indicated prolonged immune protection conferred by the constructed vaccine.

It was reported that the mRNA vaccines made by Pfizer-BioNTech and Moderna caused effective IgG responses and produced numerous memory B cells (Polack et al., 2020; Baden et al., 2021). The current candidate vaccine exhibited a similar pattern, with a rapid IgG1 response and long-lasting memory B cells, suggesting that the immune response may persist over time. Regarding B cells expressing isotypes, IgM-expressing B cells are part of the primary immune response. Their persistence indicates the continued presence of antigens or immune boosting. Similar trends are observed in the vector-based Johnson and Johnson COVID-19 vaccine (Ad26.COV2.S), where IgM lasts longer before class switching (Sadoff et al., 2021). Comparable macrophage activation trends have been noted in mRNA vaccines (Baden et al., 2021) and protein-based vaccines (Heath et al., 2021), supporting robust immune priming. The present vaccine demonstrated a rapid increase in total TH cells and memory T-helper cells. Similar to the BNT162b2 and mRNA-1273 vaccines, which exhibited the induction of a robust Th1-skewed response essential for viral elimination (Polack et al., 2020). The designed vaccine elicited dendritic cells (DCs), which efficiently drive antigen-specific T cell activation. Effective DC activation is crucial for mRNA vaccine-induced immunity (Tarke et al., 2021). IFN-γ is essential for Th1 polarization, which enhances cytotoxic T-cell (CD8+) activity and facilitates pathogen elimination. The present vaccine induced a strong IFN-γ response, indicating the activation of cell-mediated immunity. This discovery is analogous to mRNA vaccines (Pfizer/Moderna) and viral vector vaccines (AstraZeneca) (Sahin et al., 2021; Sadoff et al., 2021). The designed vaccine increased interleukin IL-2, which showed that it could cause T-cells to grow and differentiate, which would lead to a strong immune response. This trend has been observed in mRNA vaccines, which

have induced early T-cell proliferation for enhanced immunity (Mudd et al., 2022). Furthermore, the immune simulation results indicated that IL-10 was released, resulting in a vaccination with reduced side effects. This cytokine helps the immune system heal and lower inflammation (Voysey et al., 2021).

The codon optimization tool in VecBuilder yielded favorable results, achieving a CAI of 0.91 and a GC content of 59.92%, thereby satisfying the optimal expression criterion for the target organism. A CAI exceeding 0.8 indicates successful expression (Morla and Kumar, 2016), while a GC concentration between 30% and 70% is advised for optimal gene expression in the chosen organism (SignaGen Laboratories, 2015). Multiple studies have demonstrated that immunoinformatics techniques can be employed to develop and evaluate vaccines for various targets (Mahmoudvand et al., 2022; Shawan et al., 2022; Sanami et al., 2023; Shahab et al., 2023). Overall, the findings indicated that the chimeric vaccine construct is robust, efficacious, safe, and capable of concurrently halting numerous pandemics through *in silico* analysis. However, it is advisable to validate this vaccine candidate both *in vitro* and *in vivo* to ensure safety and efficacy.

CONCLUSION

Papillomaviruses are non-enveloped viruses with circular, double-stranded DNA, capable of infecting both humans and companion animals. Human papillomavirus infections persist due to limited preventative vaccinations targeting specific species. The immunoinformatics approach enables the rapid and cost-effective development of broad-spectrum mRNA vaccines against human papillomaviruses, showing promise for addressing papillomavirus infections in humans, as well as animals, including livestock and pets. This study demonstrated that the proposed mRNA-based vaccine design is highly efficient and induces immune responses through *in silico* immunological simulation. Furthermore, the vaccine's physicochemical properties indicated that it is soluble and stable, possesses a strong affinity for binding to innate immunological receptors (TLRs), and demonstrates flexible, durable, and adaptable dynamic interatomic interactions. These characteristics suggested that the vaccine can support both innate and adaptive immunity against specific viral infections. The proposed vaccine design is a promising contender for producing mRNA vaccines for global use. The design of a potentially wide-spectrum vaccine is a significant step forward in vaccine research and pandemic preparedness. Despite the encouraging findings of the present study, more *in vitro* and *in vivo* experimental testing is advised to confirm its safety and effectiveness.

DECLARATIONS

Acknowledgments

The authors extend their gratitude to the African Union Commission for the support provided through the Pan African Union and the Pan African University Institute for Basic Sciences, Technology, and Innovation (PAUSTI), Kenya.

Authors' contributions

Nshimiyimana Sylvere, James Kimotho, and Caroline Wangari Ngugi contributed to the conceptualization of the study, software development, investigation, resource acquisition, writing review and editing, project administration, and funding acquisition. Nshimiyimana Sylvere contributed to the methodology, validation, formal analysis, data curation, writing original draft preparation, and visualization. James Kimotho and Caroline Wangari Ngugi contributed to the supervision of the study. The manuscript content was reviewed and checked by all authors.

Competing interests

The authors declared no conflict of interest.

Availability of data and materials

The original data presented in the study are available in the article.

Funding

This study was supported by the African Union Commission through the Pan African University Institute for Basic Sciences, Technology, and Innovation (PAUSTI), Kenya.

Ethical considerations

Ethical issues, including plagiarism, consent to publish, misconduct, data fabrication and/or falsification, double publication and submission, and redundancy, have been checked by all authors.

REFERENCES

Ahmed HG, Bensumaidea SH, Alshammari FD, Alenazi HFS, ALmutlaq BA, Alturkstani MZ, and Aladani IA (2017). Prevalence of human papillomavirus subtypes 16 and 18 among Yemeni patients with cervical cancer. Asian Pacific Journal of Cancer Prevention, 18(6): 1543-1548. DOI: https://www.doi.org/10.22034/APJCP.2017.18.6.1543

Akbay B, Abidi SH, Ibrahim MAA, Mukhatayev Z, and Ali S (2021). Multi-subunit sars-cov-2 vaccine design using evolutionarily conserved T-and B-cell epitopes. Vaccines, 9(7): 70-72. DOI: https://www.doi.org/10.3390/vaccines9070702

Akuzum B, Kim S, Nguyen TT, Hong J, Lee S, Kim E, Kim J, Choi Y, Jhun H, Lee Y et al. (2018). L1 recombinant proteins of HPV tested for antibody forming using sera of HPV quadrivalent vaccine. Immune Network, 18(3): 1-13. DOI: https://www.doi.org/10.4110/in.2018.18.e19

Baden LR, El Sahly HM, Essink B, Kotloff K, Frey S, Novak R, Diemert D, Spector SA, Rouphael N, Creech CB et al. (2021). Efficacy and safety of the mRNA-1273 SARS-CoV-2 vaccine. New England journal of medicine, 384(5): 403-16. DOI: https://www.doi.org/10.1016/j.colsurfb.2025.114598

Boxus M, Fochesato M, Miseur A, Mertens E, Dendouga N, Brendle S, Balogh KK, Christensen ND, and Giannini SL (2016). Broad cross-protection is induced in preclinical models by a human papillomavirus vaccine composed of L1/L2 chimeric virus-like particles. Journal of Virology, 90(14): 6314-6325. DOI: https://www.doi.org/10.1128/jvi. 00449-16

Bruni L, Diaz M, Castellsagué X, Ferrer E, Bosch FX, and De Sanjosé S (2010). Cervical human papillomavirus prevalence in 5 continents: Meta-analysis of 1 million women with normal cytological findings. Journal of Infectious Diseases, 202(12): 1789-1799. DOI: https://www.doi.org/10.1086/657321

Cai H, Feng Y, Fan P, Guo Y, Kuerban G, Chang C, and Wang R (2021). HPV16 E6-specific T cell response and HLA-A alleles are related to the prognosis of patients with cervical cancer. Infectious Agents and Cancer, 16: 1-11. DOI: https://www.doi.org/10.1186/s13027-021-00395-y

Castro F, Cardoso AP, Gonçalves RM, Serre K, and Oliveira MJ (2018). Interferon-gamma at the crossroads of tumor immune surveillance or evasion. Frontiers in Immunology, 9: 847. DOI: https://www.doi.org/10.3389/fimmu.2018.00847

Chen X, Zaro JL, and Shen WC (2013). Fusion protein linkers: property, design and functionality. Advanced Drug Delivery Reviews, 65(10): 1357-69. DOI: https://www.doi.org/10.1016/j.addr.2012.09.039

Chesson HW, Ekwueme DU, Saraiya M, Watson M, Lowy DR, and Markowitz LE (2012). Estimates of the annual direct medical costs of the prevention and treatment of disease associated with human papillomavirus in the United States. Vaccine, 30(42): 6016-6019. DOI: https://www.doi.org/10.1016/j.vaccine.2012.07.056

Dehghani A, Mamizadeh M, Karimi A, Hosseini SA, Siamian D, Shams M, Ghiabi S, Basati G, and Abaszadeh A (2024). Multi-epitope vaccine design against leishmaniasis using IFN-γ inducing epitopes from immunodominant gp46 and g63 proteins. Journal of Genetic Engineering and Biotechnology, 22(1): 100355. DOI: https://www.doi.org/10.1016/ j.jgeb.2024.100355

Dimitrov I, Bangov I, Flower DR, and Doytchinova I (2014). AllerTOP v.2 - a server for *in silico* prediction of allergens. Journal of Molecular Model, 20: 2278. DOI: https://www.doi.org/10.1007/s00894-014-2278-5

Du Z, Su H, Wang W, Ye L, Wei H, Peng Z, Anishchenko, I, Baker D, and Yang J (2021). The trRosetta server for fast and accurate protein structure prediction. Nature Protocols, 16(12): 5634-5651. DOI: https://www.doi.org/10.1038/s41596-021-00628-9

Geraets D, Alemany L, Guimera N, De Sanjose S, De Koning M, Molijn A, Jenkins D, Bosch X, and Quint W (2012). Detection of rare and possibly carcinogenic human papillomavirus genotypes as single infections in invasive cervical cancer. Journal of Pathology, 228(4): 534-543. DOI: https://www.doi.org/10.1002/path.4065

Ghaffari-Nazari H, Tavakkol-Afshari J, Jaafari MR, Tahaghoghi-Hajghorbani S, Masoumi E, and Jalali SA (2015). Improving multi-epitope long peptide vaccine potency by using a strategy that enhances CD4+ T help in BALB/c mice. PLoS ONE, 10(11): e0142563. DOI: https://www.doi.org/10.1371/journal.pone.0142563

Ghorban Hosseini N, Tebianian M, Farhadi A, Hossein Khani A, Rahimi A, Mortazavi M, Hosseini SY, Taghizadeh M, Rezaei M, and Mahdavi M (2017). *In silico* analysis of L1/L2 sequences of human papillomaviruses: Implication for universal vaccine design. Viral Immunology, 30(3): 210-223. DOI: https://www.doi.org/10.1089/vim.2016.0142

Gruber A R, Lorenz R, Bernhart SH, Neuböck R, and Hofacker IL (2008). The Vienna RNA websuite. Nucleic Acids Research, 36: 70-74. DOI: https://www.doi.org/10.1093/nar/gkn188

Guan P, Qi C, Xu G, Sheng C, Sun S, Zhou Z, and Jia S (2025). Designing a T cell multi-epitope vaccine against hRSV with reverse vaccinology: An immunoinformatics approach. Colloids and Surfaces B: Biointerfaces, 251: 114599. DOI: https://www.doi.org/10.1016/j.colsurfb.2025.114599

Gupta S, Kapoor P, Chaudhary K, Gautam A, Kumar R, and Raghava GPS (2013). *In silico* approach for predicting toxicity of peptides and proteins. PLoS ONE, 8(9): e73957. DOI: https://www.doi.org/10.1371/journal.pone.0073957

Gurunathan S, Klinman DM, and Seder RA (2000). DNA vaccines: Immunology, application, and optimization. Annual Review of Immunology, 18(1): 927-74. DOI: https://www.doi.org/10.1146/annurev.immunol.18.1.927

Heath PT, Galiza EP, Baxter DN, Boffito, Browne D, Burns F, and Toback S (2021). Safety and efficacy of NVX-CoV2373 Covid-19 vaccine. New England Journal of Medicine, 385(13): 1172-1183. DOI: https://www.doi.org/10.1016/j.ebiom.2025.105634

Hebditch M, Carballo-Amador MA, Charonis S, Curtis R, and Warwicker J (2017). Protein–sol: A web tool for predicting protein solubility from sequence. Bioinformatics, 33(19): 3098-3100. DOI: https://www.doi.org/10.1093/ bioinformatics/btx345

Haręża DA, Wilczyński JR, and Paradowska E (2022). Human papillomaviruses as infectious agents in gynecological cancers—oncogenic properties of viral proteins. International Journal of Molecular Sciences, 23(3): 1818. DOI: https://www.doi.org/10.3390/ijms23031818

Hasan M, Ahmed S, Imranuzzaman M, Bari R, Roy S, Hasan MM, and Mia MM (2024). Designing and development of efficient multi-epitope-based peptide vaccine candidate against emerging avian rotavirus strains: A vaccinomic approach. Journal of Genetic Engineering and Biotechnology, 22(3): 100398. DOI: https://www.doi.org/10.1016/j.jgeb.2024.1 00398

Huber B, Wang JW, Roden RBS, and Kirnbauer R (2021). Rg1-vlp and other l2-based, broad-spectrum hpv vaccine candidates. Journal of Clinical Medicine, 10(5): 1044. DOI: https://www.doi.org/10.3390/jcm10051044

Kakakhel S, Ahmad A, Mahdi WA, Alshehri S, Aiman S, Begum S, Shams S, Kamal M, Imran M, Shakeel F et al. (2023). Annotation of potential vaccine targets and designing of mRNA-based multi-epitope vaccine against lumpy skin disease virus via reverse vaccinology and agent-based modeling. Bioengineering, 10(4): 430. DOI: https://www.doi.org/10.3390/bioengineering10040430

Kowalzik F, Schreiner D, Jensen C, Teschner D, Gehring S, and Zepp F (2021). mRNA-based vaccines. Vaccines, 9(4): 390. DOI: https://www.doi.org/10.3390/vaccines9040390

Kumar A, Sahu U, Kumari P, Dixit A, and Khare P (2022). Designing of multi-epitope chimeric vaccine using immunoinformatic platform by targeting oncogenic strain HPV 16 and 18 against cervical cancer. Scientific Reports, 12(1): 9521. DOI: https://www.doi.org/10.1038/s41598-022-13442-4

Jagu S, Malandro N, Kwak K, Yuan H, Schlegel R, Palmer KE, Huh WK, Campo MS, and Roden RB (2011). A multimeric L2 vaccine for prevention of animal papillomavirus infections. Virology, 420(1): 43-50. DOI: https://www.doi.org/10.1016/j.virol.2011.07.020

Jedy-Agba E, Joko WY, Liu B, Buziba NG, Borok M, Korir A, Masamba L, Manraj SS, Finesse A, Wabinga H et al. (2020). Trends in cervical cancer incidence in sub-Saharan Africa. British Journal of Cancer, 123(1): 148-154. https://www.doi.org/10.1038/s41416-020-0831-9

Jensen KK, Andreatta M, Marcatili P, Buus S, Greenbaum JA, Yan Z, Sette A, Peters B, and Nielsen M (2018). Improved methods for predicting peptide binding affinity to MHC class II molecules. Immunology, 154(3): 394-406. DOI: https://www.doi.org/10.1111/imm.12889

Jin L, Zhou Y, Zhang S, and Chen SJ (2025). mRNA vaccine sequence and structure design and optimization: Advances and challenges. Journal of Biological Chemistry, 301(1): 108015. DOI: https://www.doi.org/10.1016/j.jbc.2024.108015

Lampe AT, Puniya BL, Pannier AK, Helikar T, and Brown DM (2020). Combined TLR4 and TLR9 agonists induce distinct phenotypic changes in innate immunity *in vitro* and *in vivo*. Cellular immunology, 355:104149. DOI: https://www.doi.org/10.1016/j.cellimm.2020.104149

Larsen MV, Lundegaard C, Lamberth K, Buus S, Lund O, and Nielsen M (2007). Large-scale validation of methods for cytotoxic T-lymphocyte epitope prediction. BMC Bioinformatics, 8: 424. Available at: https://bmcbioinformatics.biomedcentral.com/articles/10.1186/1471-2105-8-424

Lee YR, Liou CW, Liu IH, and Chang JM (2024). A nonadjuvanted HLA-restricted peptide vaccine induced both T and B cell immunity against SARS-CoV-2 spike protein. Scientific Reports, 14(1): 20579. DOI: https://www.doi.org/10.1038/s41598-024-71663-1

Li L, Guo Y, Li Z, Zhou Y, and Zeng Y (2016). Protein transduction domain can enhance the humoral immunity and cross-protection of HPV16L2 peptide vaccines. Biomedical Reports, 4(6): 746-750. DOI: https://www.doi.org/10.3892/br.2016.647

Li M, Wang H, Tian L, Pang Z, Yang Q, Huang T, Fan J, Song L, Tong Y, and Fan H (2022). COVID-19 vaccine development: milestones, lessons and prospects. Signal transduction and Targeted Therapy, 7(1): 146. DOI: https://www.doi.org/10.1038/s41392-022-00996-y

Liu Y, Yang Q, and Zhao F (2021). Synonymous but not silent: The codon usage code for gene expression and protein folding. Annual Review of Biochemistry, 90: 375-401. DOI: https://www.doi.org/10.1146/annurev-biochem-071320-112701

Lon JR, Bai Y, Zhong B, Cai F, and Du H (2020). Prediction and evolution of B cell epitopes of surface protein in SARS-CoV-2. Virology Journal, 1-9. DOI: https://www.doi.org/10.1186/s12985-020-01437-4

López-Blanco JR, Aliaga JI, Quintana-Ortí ES, and Chacón P (2014). IMODS: Internal coordinates normal mode analysis server. Nucleic Acids Research, 42(W1): 271-276. DOI: https://www.doi.org/10.1093/nar/gku339

Kaur A, Baldwin J, Brar D, Salunke DB, and Petrovsky N (2022). Toll-like receptor (TLR) agonists as a driving force behind next-generation vaccine adjuvants and cancer therapeutics. Current Opinion in Chemical Biology, 70: 102172. DOI: https://www.doi.org/10.1016/j.cbpa.2022.102172

Mahmoodi S, Amirzakaria JZ, and Ghasemian A (2023). *In silico* design and validation of a novel multiepitope vaccine candidate against structural proteins of Chikungunya virus using comprehensive immunoinformatics analyses. PLoS ONE, 18(5): e0285177. DOI: https://www.doi.org/10.1371/journal.pone.0285177

Mahmoudvand S, Shokri S, Makvandi M, Taherkhani R, Rashno M, Jalilian FA, and Angali KA (2022). *In silico* prediction of T-cell and B-cell epitopes of human papillomavirus type 16 L1 protein. Biotechnology and Applied Biochemistry, 69(2): 514-525. DOI: https://www.doi.org/10.1002/bab.2128

Maruggi G, Zhang C, Li J, Ulmer JB, and Yu D (2019). mRNA as a transformative technology for vaccine development to control infectious diseases. Molecular Therapy, 27(4): 757-772. DOI: https://www.doi.org/10.1016/j.ymthe. 2019.01.020

Medeiros-Fonseca B, Faustino-Rocha AI, Medeiros R, Oliveira PA, and Gil da Costa RM (2023). Canine and feline papillomaviruses: An update. Frontiers in Veterinary Science, 10: 1174673. DOI: https://www.doi.org/10.3389/fvets.2023.1174673

Mo Y, Ma J, Zhang H, Shen J, Chen J, Hong J, Xu Y, and Qian C (2022). Prophylactic and therapeutic HPV vaccines: current scenario and perspectives. Frontiers in Cellular and Infection Microbiology, 12: 909223. DOI: https://www.doi.org/10.3389/fcimb.2022.909223

Morla S, Makhija A, and Kumar S (2016). Synonymous codon usage pattern in glycoprotein gene of rabies virus. Gene, 584(1): 1-6. DOI: https://www.doi.org/10.1016/j.gene.2016.02.047

Morris AL, MacArthur MW, Hutchinson EG, and Thornton JM (1992). Stereochemical quality of protein structure coordinates. Proteins: Structure, Function, and Bioinformatics, 12(4): 345-64. DOI: https://www.doi.org/10.1002/prot.340120407

Mudd PA, Minervina AA, Pogorelyy MV, Turner JS, Kim W, Kalaidina E, and Ellebedy AH (2022). SARS-CoV-2 mRNA vaccination elicits a robust and persistent T follicular helper cell response in humans. Cell, 185(4): 603-613. DOI: https://www.doi.org/10.1016/j.cell.2021.12.026

Namvar A, Bolhassani A, Javadi G, and Noormohammadi Z (2019). *In silico*/*in vivo* analysis of high-risk papillomavirus L1 and L2 conserved sequences for development of cross-subtype prophylactic vaccine. Scientific Reports, 9(1): 15225. DOI: https://www.doi.org/10.1038/s41598-019-51679-8

Naveed M, Hassan JU, Ahmad M, Naeem N, Mughal MS, Rabaan AA, Aljeldah M, Shammari BRA, Alissa M, Sabour AA et al. (2022). Designing mRNA-and peptide-based vaccine construct against emerging multidrug-resistant Citrobacter freundii: A computational-based subtractive proteomics approach. Medicina, 58(10): 1356. DOI: https://www.doi.org/10.3390/medicina58101356

Niwa T, Ying BW, Saito K, Jin W, Takada S, Ueda T, and Taguchi H (2009). Bimodal protein solubility distribution revealed by an aggregation analysis of the entire ensemble of Escherichia coli proteins. Proceedings of the National Academy of Sciences, 106(11): 4201-4206. DOI: https://www.doi.org/10.1073/pnas.0811922106

Oladipo EK, Adeniyi MO, Ogunlowo MT, Irewolede BA, Adekanola VO, Oluseyi GS, Omilola JA, Udoh AF, Olufemi SE, Adediran DA et al. (2022). Bioinformatics designing and molecular modelling of a universal mRNA vaccine for SARS-CoV-2 infection. Vaccines, 10(12): 2107. DOI: https://www.doi.org/10.3390/vaccines10122107

Olczak P and Roden RB (2020). Progress in L2-based prophylactic vaccine development for protection against diverse human papillomavirus genotypes and associated diseases. Vaccines, 8(4): 568. DOI: https://www.doi.org/10.3390/vaccines8040568

Pichon C and Perche F. Design and delivery of messenger RNA-based vaccines. The Biochemist, 43(4): 4-7.DOI: https://www.doi.org/10.1042/bio_2021_151

Polack FP, Thomas SJ, Kitchin N, Absalon J, Gurtman A, Lockhart S, Perez JL, Pérez Marc G, Moreira ED, Zerbini C et al. (2020). Safety and efficacy of the BNT162b2 mRNA Covid-19 vaccine. New England journal of medicine, 383(27): 2603-2615. DOI: https://www.doi.org/10.1016/j.colsurfb.2025.114598

Ponomarenko J, Bui HH, Li W, Fusseder N, Bourne PE, Sette A, and Peters B (2008). ElliPro: A new structure-based tool for the prediction of antibody epitopes. BMC Bioinformatics, 9: 514. DOI: https://www.doi.org/10.1186/1471-2105-9-514

Pulendran B and Ahmed R (2011). Immunological mechanisms of vaccination. Nature Immunology, 12(6): 509-517. DOI: https://www.doi.org/10.1038/ni.2039

Rapin N, Lund O, and Castiglione F (2011). Immune system simulation online. Bioinformatics, 27(14): 2013-2014. DOI: https://www.doi.org/10.1093/bioinformatics/btr335

Rizarullah N, Aditama R, Giri-Rachman EA, and Hertadi R (2024). Designing a Novel Multiepitope Vaccine from the Human Papilloma Virus E1 and E2 Proteins for Indonesia with Immunoinformatics and Molecular Dynamics Approaches. ACS Omega, 9(14): 16547-16562. DOI: https://www.doi.org/10.1021/acsomega.4c00425

Rock KL, Reits E, and Neefjes J (2016). Present yourself by MHC class I and MHC class II molecules. Trends in Immunology, 37(11): 724-737. DOI: https://www.doi.org/10.1016/j.it.2016.08.010

Rosa DS, Tzelepis F, Cunha MG, Soares IS, and Rodrigues MM (2004). The pan HLA DR-binding epitope improves adjuvant-assisted immunization with a recombinant protein containing a malaria vaccine candidate. Immunology Letters, 92(3): 259-268. DOI: https://www.doi.org/10.1016/j.imlet.2004.01.006

Rottembourg D, Filippi CM, Bresson D, Ehrhardt K, Estes EA, Oldham JE, and von Herrath MG (2010). Essential role for TLR9 in prime but not prime-boost plasmid DNA vaccination to activate dendritic cells and protect from lethal viral infection. The Journal of Immunology, 184(12): 7100-71007. DOI: https://www.doi.org/10.4049/jimmunol.0803935

Ryan N, Pratiwi SE, Mardhia M, Ysrafil Y, Liana DF, and Mahyarudin M (2024). Immunoinformatics approach for design novel multiepitope prophylactic and therapeutic vaccine based on capsid proteins L1 and L2 and oncoproteins E6 and E7 of human papillomavirus 16 and human

papillomavirus 18 against cervical cancer. Osong Public Health and Research Perspectives, 15(4): 307-328. DOI: https://www.doi.org/10.24171/j.phrp.2024.0013

Sadoff J, Le Gars M, Shukarev G, Heerwegh D, Truyers C, de Groot AM, Stoop J, Tete S, Van Damme W, Leroux-Roels I et al. (2021). Interim results of a phase 1-2a trial of Ad26. COV2. S Covid-19 vaccine. New England Journal of Medicine, 384(19): 1824-1835. DOI: https://www.doi.org/10.1056/NEJMoa2034201

Saha S and Raghava GPS (2006). Prediction of Continuous B-cell Epitopes in an Antigen Using Recurrent Neural Network. Proteins, 65(1): 40-48. DOI: https://www.doi.org/10.1002/prot.21078

Sahin U, Muik A, Vogler I, Derhovanessian E, Kranz LM, Vormehr M, Quandt J, Bidmon N, Ulges A, Baum A et al. (2021). BNT162b2 vaccine induces neutralizing antibodies and poly-specific T cells in humans. Nature, 595(7868): 572-577. DOI: https://www.doi.org/10.1038/s41586-021-03653-6

Sanami S, Nazarian S, Ahmad S, Raeisi E, ul Qamar MT, Tahmasebian S, Pazoki-Toroudi H, Fazeli M, and Ghatreh Samani M (2023). *In silico* design and immunoinformatics analysis of a universal multi-epitope vaccine against monkeypox virus. PLoS ONE, 18(5): e0286224. DOI: https://www.doi.org/10.1371/journal.pone.0286224

Serretiello E, Corrado F, Santella B, Chianese A, Iervolino D, Coppola A, Grimaldi E, Galdiero M, and Franci G (2023). Prevalence and distribution of high- and low- risk HPV genotypes in women living in the Metropolitan Area of Naples: A recent update. Asian Pacific Journal of Cancer Prevention, 24(2): 435-441. DOI: https://www.doi.org/10.31557 /APJCP.2023.24.2.435

Sha T, Li Z, Zhang C, Zhao X, Chen Z, Zhang F, and Ding J (2020). Bioinformatics analysis of candidate proteins Omp2b, P39 and BLS for Brucella multivalent epitope vaccines. Microbial Pathogenesis, 147: 104318. DOI: https://www.doi.org/10.1016/j.micpath.2020.104318

Shahab M, Guo D, Zheng G, and Zou Y (2023). Design of a novel and potent multi-epitope chimeric vaccine against human papillomavirus (HPV): An immunoinformatics approach. Biomedicines, 11(5): 1493. DOI: https://www.doi.org/10.3390/biomedicines11051493

Shao S, Risch E, Burner D, Lu L, Minev B, and Ma W (2017). IFNγ enhances cytotoxic efficiency of the cytotoxic T lymphocytes against human glioma cells. International Immunopharmacology, 47: 159-165. DOI: https://www.doi.org/10.1016/j.intimp.2017.04.003

Shawan MMAK, Sharma AR, Halder SK, Arian TAl, Shuvo MN, Sarker SR, and Hasan MA (2023). Advances in computational and bioinformatics tools and databases for designing and developing a multi-epitope-based peptide vaccine. International Journal of Peptide Research and Therapeutics, 29(4): 60. DOI: https://www.doi.org/10.1007/s10989-023-10535-0

SignaGen laboratories (2015). Good transgene expression measured by CAI. Available at: https://signagen.com/blog/2015/10/30/good-transgene-expression-measured-by-cai

Shi J, Zhu Y, Yin Z, He Y, Li Y, Haimiti G, Xie X, Niu C, Guo W, and Zhang F (2024). *In silico* designed novel multi-epitope mRNA vaccines against Brucella by targeting extracellular protein BtuB and LptD. Scientific Reports, 14(1): 7278. DOI: https://www.doi.org/10.1038/s41598-024-57793-6

Singh D, Vignat J, Lorenzoni V, Eslahi M, Ginsburg O, Lauby-Secretan B, Arbyn M, Basu P, Bray F, and Vaccarella S (2023). Global estimates of incidence and mortality of cervical cancer in 2020: A baseline analysis of the WHO Global Cervical Cancer Elimination Initiative. The Lancet Global Health, 11(2): e197-e206. DOI: https://www.doi.org/10. 1016/S2214-109X(22)00501-0

Soltan MA, Elbassiouny N, Gamal H, Elkaeed EB, Eid RA, Eldeen MA, and Al-Karmalawy AA (2021). *In silico* prediction of a multitope vaccine against Moraxella catarrhalis: reverse vaccinology and immunoinformatics. Vaccines, 9(6): 669. DOI: https://www.doi.org/10.3390/vaccines9060669

Sun H, Zhang Y, Wang G, Yang W, and Xu Y (2023). mRNA-based therapeutics in cancer treatment. Pharmaceutics, 15(2): 622. DOI: https://www.doi.org/10.3390/pharmaceutics15020622

Tarke A, Sidney J, Methot N, Yu ED, Zhang Y, Dan JM, Goodwin B, Rubiro P, Sutherland A, Wang E et al. (2021). Impact of SARS-CoV-2 variants on the total CD4+ and CD8+ T cell reactivity in infected or vaccinated individuals. Cell Reports Medicine, 2(7): 100355. DOI: https://www.doi.org/10.1016/j.xcrm.2021.100355

Tarrahimofrad H, Rahimnahal S, Zamani J, Jahangirian E, and Aminzadeh S (2021). Designing a multi-epitope vaccine to provoke the robust immune response against influenza A H7N9. Scientific Reports, 11(1): 24485. DOI: https://www.doi.org/10.1038/s41598-021-03932-2

Ullah N, Anwer F, Ishaq Z, Siddique A, Shah MA, Rahman M, Rahman A, Mao X, Jiang T, Lee BL et al. (2022 *In silico* designed Staphylococcus aureus B-cell multi-epitope vaccine did not elicit antibodies against target antigens suggesting multi-domain approach. Journal of Immunological Methods, 504: 113264. DOI: https://www.doi.org/10.1016/j.jim.2022.113264

Verbeke R, Hogan M J, Loré K, and Pardi N (2022). Innate immune mechanisms of mRNA vaccines. Immunity, 55(11): 1993-2005. DOI: https://www.doi.org/10.1016/j.immuni.2022.10.014

Voysey M, Clemens SA, Madhi SA, Weckx LY, Folegatti PM, Aley PK, Angus B, Baillie VL, Barnabas SL, Bhorat QE et al. (2021). Safety and efficacy of the ChAdOx1 nCoV-19 vaccine (AZD1222) against SARS-CoV-2: an interim analysis of four randomised controlled trials in Brazil, South Africa, and the UK. Lancet, 397(10269): 99-111. DOI: https://www.doi.org/10.1016/S0140-6736(20)32661-1

Wang JW (2015). Immunology and vaccinology of human papillomavirus minor capsid protein L2. Doctoral dissertation, Johns Hopkins University, Baltimore, Maryland.

Ward AB and Wilson IA (2020). Innovations in structure-based antigen design and immune monitoring for next generation vaccines. Current Opinion in Immunology, 65: 50-56. DOI: https://www.doi.org/10.1016/j.coi.2020.03.013

Waterhouse AM, Procter JB, Martin DMA, Clamp M, and Barton GJ (2009). Jalview Version 2-A multiple sequence alignment editor and analysis workbench. Bioinformatics, 25(9): 1189-1191. DOI: https://www.doi.org/10.1093/ bioinformatics/btp033

Wiederstein M and Sippl MJ (2007). ProSA-web: interactive web service for the recognition of errors in three-dimensional structures of proteins. Nucleic Acids Research, 35(suppl 2): W407-W410. DOI: https://www.doi.org/10.1093/nar/gkm290